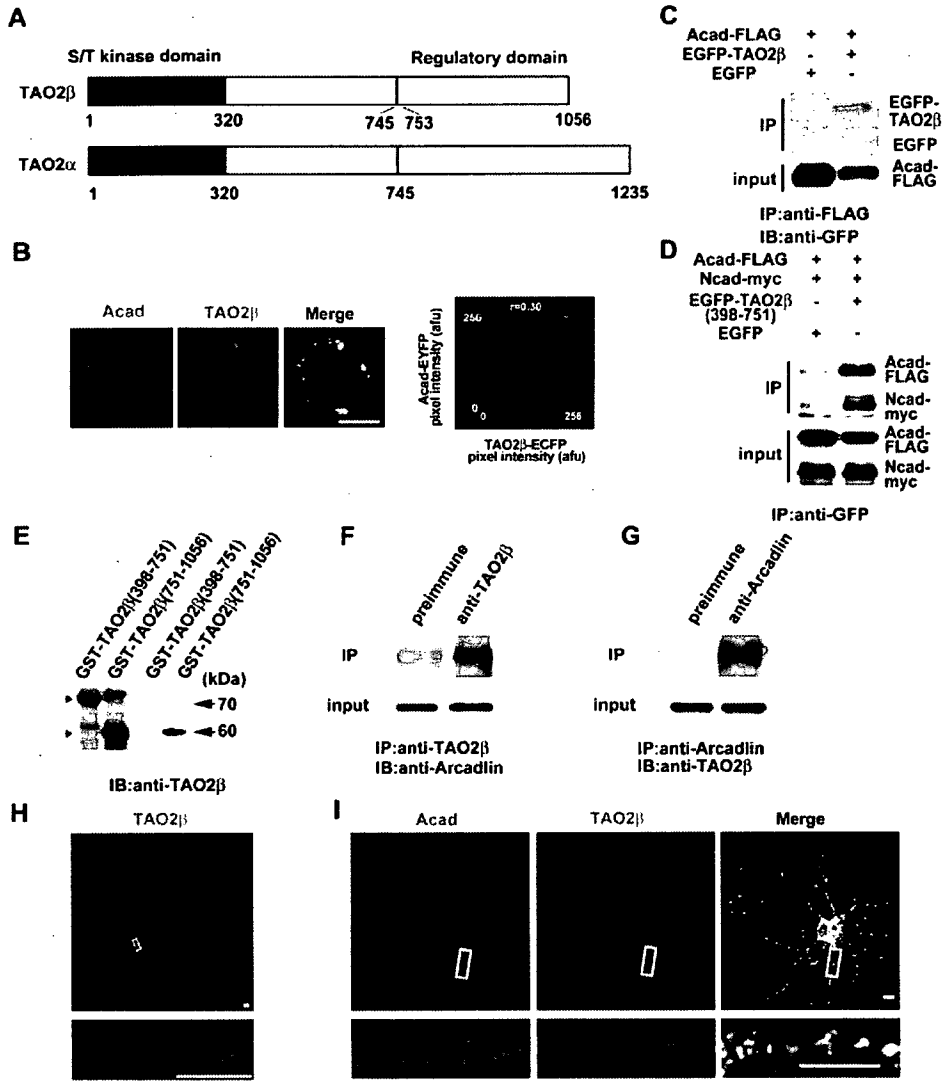

Figure 4. TAO2β Binds to the Intracellular Domain of Arcadlin

(A) Diagram of TAO2 kinases. An isoform of TAO2 (TAO2β) was identified as an intracellular binding partner of arcadlin. The original TAO2 was renamed as TAO2α. Most of the C-terminal regulatory domain of TAO2β (aa 753–1056) is distinct from that of TAO2α.

(B) Typical fluorescence image (left) and scatterplot (right) of HEK293T cells coexpressing TAO2β-ECFP and arcadlin-EYFP. Significant colocalization confirmed ($r = 0.30$).

(C) Arcadlin-FLAG was immunoprecipitated (IP) from HEK293T cells transfected with *arcadlin-flag* and *EGFP-tao2β* and immunoblotted (IB) with anti-GFP serum.

(D) EGFP-TAO2β(398-751) or control EGFP was immunoprecipitated with anti-GFP serum (IP) from HEK293T cells transfected with *arcadlin-flag*, *N-cadherin-myc*, and *EGFP-tao2β(398–751)* and immunoblotted for arcadlin (anti-FLAG) and N-cadherin (anti-myc). Left, transfected with *EGFP* instead of *EGFP-tao2β(398–751)*.

(E) The affinity purified anti-TAO2β antibody recognized the unique regulatory domain specific for the β isoform. Left, CBB protein staining.

(F) Hippocampal extract immunoprecipitated with anti-TAO2β antibody and immunoblotted for arcadlin.

(G) Hippocampal extract immunoprecipitated with anti-arcadlin antibody and immunoblotted for TAO2β.

(H) Cultured neurons were immunostained for TAO2β.

(I) Confocal live imaging of arcadlin-EYFP (green) and TAO2β-ECFP (red) expressed in dendrites.

Scale bars, 10 μm.

suggesting that *tao2α* and -β mRNAs are alternative splicing products from the same gene (Figure S2A).

A recombinant TAO2β tagged at its carboxyl terminus with enhanced cyan fluorescent protein (TAO2β-ECFP) colocalized with arcadlin-EYFP (enhanced yellow fluorescent protein) in HEK293T cells (Figure 4B). The molecular interaction between these proteins was confirmed by coimmunoprecipitation (Figure 4C). The formation of a

trimeric complex of TAO2β, arcadlin, and N-cadherin was confirmed in triple-transfected HEK293T cells (Figure 4D). The association of EGFP-TAO2β (398–751), the central domain common to both α and β isoforms, suggested that TAO2α can also bind to arcadlin (Figure 4D). In order to examine in vivo interactions of TAO2β, we produced and purified a polyclonal antibody recognizing the carboxy-terminal domain specific for the β isoform of TAO2 kinase (Figure 4E). Coimmunoprecipitation of endogenous arcadlin protein with the anti-TAO2β antibody (Figure 4F) and, reciprocally, of TAO2β with anti-arcadlin antibody (Figure 4G) confirmed that these molecules associate in vivo in MECS-treated rat hippocampi. Immunolocalization of TAO2β showed puncta in dendrites (Figure 4H). Arcadlin-EYFP and TAO2β-ECFP transfected into cultured hippocampal neurons colocalized in dendrites (Figure 4I). We conclude that the arcadlin protocadherin and the TAO2β MAPKKK interact in hippocampal neurons.

Arcadlin Homophilic Interaction Triggers Activation of p38 MAPK and Internalization

The arcadlin/PAPC extracellular domain mediates homophilic binding (Chen and Gumbiner, 2006; Kim et al., 1998; Yamagata et al., 1999). In addition, arcadlin is a transiently expressed protein in hippocampal neurons, whose protein level peaks at 4 hr after the synaptic stimulation and largely disappears within 8 hr (Yamagata et al., 1999). During this period, the arcadlin protein is transported to pre- and postsynaptic membranes and rapidly turned over (Yamagata et al., 1999). In HEK293T cells cotransfected with *arcadlin-EGFP* and *arcadlin-flag*, arcadlin-arcadlin lateral interactions in the same membrane were readily detectable (Figure 5A, lane3). To analyze *trans* interactions specifically, we utilized arcadlin-L, a splice variant of arcadlin containing a 98 amino acid insertion in its cytoplasmic region. Arcadlin-L-EGFP-expressing cells and arcadlin-L-FLAG-expressing cells were cocultured so that these two types of cells attached to each other. Immunoprecipitation of arcadlin-L-EGFP with anti-flag antibody indicated that there is significant binding activity in *trans* (Figure 5A, lane 1). Application of a soluble extracellular fragment of recombinant arcadlin protein (Acad-EC, purified via a His-tag) into the culture medium competed *trans*-association, indicating that Acad-EC binds to the extracellular domain of arcadlin in *trans* (Figure 5A, lane 2). Although *cis* interaction may be also involved, Acad-EC at this concentration was not sufficient to replace the lateral oligomerization (data not shown).

Arcadlin molecules expressed in HEK293T cells abundantly localized to the cell surface. There was also detectable fraction of arcadlin in intracellular vesicles (Figure 5B, 0 min). Homophilic interaction of arcadlin on the cell surface with Acad-EC added to the culture medium triggered the rapid translocation of arcadlin from the periphery to the center of HEK293T cells cotransfected as described below (Figure 5B). This shift is mediated by endocytosis, because the moved arcadlin colocalized with EGFP-rab5 as a marker for endosomes and because the internalization of arcadlin was blocked by a coexpression of a dominant-negative form of dynamin, as shown in Figures 5B and 5G. A similar endocytic response was observed upon the application of the antibody against the extracellular region of arcadlin (data not shown). Therefore, a binding of the extracellular domain is sufficient to enhance the endocytosis of arcadlin. We next used this Acad-EC reagent to investigate the signal transduction mechanism that triggers endocytosis. It should be noted that a detectable level of background arcadlin endocytosis before the addition of Acad-EC may be triggered by the *cis* homophilic interaction of the transfected arcadlin (Figure 5B, 0 min).

Because TAO2β forms a molecular complex with the arcadlin intracellular domain, we asked whether p38 MAPK, a main target kinase of the TAO2α-MAPKKK pathway bridged by MEK3 (MAPKK-3) (Chen et al., 2003), was activated by the arcadlin signal. HEK293T cells cotransfected with *arcadlin*, *tao2β*, *MEK3*, and *p38 MAPK* were treated by addition of purified Acad-EC (10 μg/ml) to the culture medium. Immunostaining and immunoblot of the phosphorylated forms of p38 MAPK and MEK3 revealed that the phosphorylation levels of both kinases were enhanced within 30 min of the application of Acad-EC (Figures 5B and 5C). The p38 MAPK phosphorylation is mediated by arcadlin and TAO2β, because Acad-EC did not exert any response in HEK293T cells lacking either *arcadlin* or *tao2β* transfection (Figure 5D). Importantly, addition of Acad-EC protein triggered the activation of endogenous p38 MAPK in the dendritic shaft of primary cultures of rat hippocampal neurons (Figure 5E). Taken together, the results suggest that the arcadlin extracellular domain activates p38 MAPK via TAO2β. In cultured neurons, activation of p38 was detected specifically in the dendritic shaft after addition of protocadherin extracellular domain.

TAO2β Is Required for p38 Activation and Endocytosis of Arcadlin

We then addressed whether TAO2β is necessary for the phosphorylation of p38 MAPK and the endocytosis of arcadlin. We reconstituted the arcadlin-TAO2β-MEK3-p38 MAPK signaling pathway in HEK293T cells by cotransfecting *arcadlin* with *tao2β*, *tao2βK57A* (catalytically defective TAO2 kinase; Chen et al., 2003), or *tao2α*. After the treatment with Acad-EC for 30 min, cells were analyzed for the phosphorylation of p38 MAPK (Figure 5F) and endocytosis of arcadlin by the surface biotinylation assay (Figure 5G). The phosphorylation of p38 MAPK was significantly increased, and surface arcadlin levels were significantly reduced in cells expressing wild-type TAO2β (Figures 5F and 5G). In *mock* or *tao2βK57A*-transfected cells, neither the endocytosis of arcadlin nor the phosphorylation of p38 MAPK was observed (Figures 5F and 5G). Cells expressing TAO2α displayed full activation of p38 MAPK but were deficient in the internalization of arcadlin (Figures 5F and 5G). We conclude from these data that the kinase

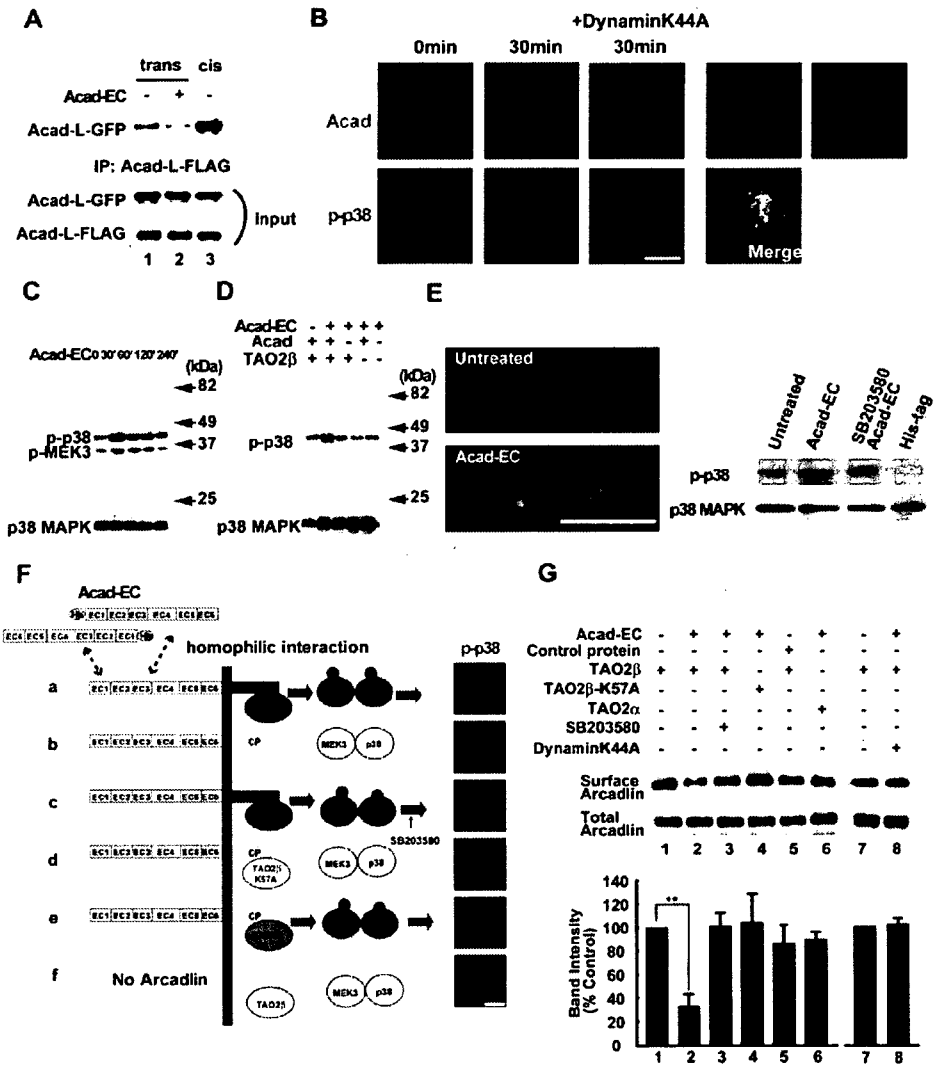

Figure 5. Homophilic Interaction of Arcadlin Causes Internalization via the Activation of Arcadlin-TAO2β-p38 MAPK Signaling Pathway

(A) Arcadlin-L-GFP or arcadlin-L-FLAG were expressed on different cell surfaces independently and allowed to interact across the cell-cell junction in mixed cell culture and were immunoprecipitated with anti-FLAG antibody followed by immunoblot for GFP (top). Bottom, input. Acad-EC protein added in the culture medium inhibited the *trans*-interaction (lane 2, compared with lane 1). Lane 3, cotransfection of *arcadlin-l-EGFP* and *arcadlin-l-flag*, which allows *cis*-interaction.

(B) HEK293T cells transfected with *arcadlin*, *tao2β*, *MEK3*, and *p38 MAPK* were treated with Acad-EC (10 μg/ml, 30 min) and immunostained. *dynaminK44A* (center) or *EGFP-rab5* (right) was additionally cotransfected. Surface and cytoplasmic localizations were revealed by optical sectionings by a confocal microscope.

(C) Extracts of HEK293T cells transfected with *arcadlin*, *tao2β*, *MEK3*, and *p38 MAPK* and treated with Acad-EC were immunoblotted for phospho-p38 MAPK and phospho-MEK3.

(D) Extracts of HEK293T cells with or without transfection of *arcadlin* and *tao2β* were immunoblotted for p38 phosphorylation upon the addition of Acad-EC to culture medium.

(E) Cultured hippocampal neurons at 18 DIV pretreated with IBMX and forskolin were treated with Acad-EC (10 μg/ml) for 30 min followed by immunostaining (left) for arcadlin (green) and phospho-p38 MAPK (red); corresponding immunoblot shown to the right.

(F) Reconstitution of the arcadlin-TAO2β-p38 MAPK pathway in HEK293T cells transfected as described. Cells in (C) were pretreated with 10 μM SB203580. Cells were treated with Acad-EC for 30 min and immunostained for phospho-p38 MAPK.

(G) Quantification of surface arcadlin level by biotinylation method in HEK293T cells transfected and treated as indicated. Densitometric quantification from five separate experiments is summarized in histogram (mean ± SEM).

**$p < 0.01$. Scale bars, 10 μm.

activity of TAO2α and -β that resides in their common catalytic domains is sufficient for the phosphorylation and activation of p38 MAPK. The endocytosis of arcadlin, however, depends exclusively on TAO2β, suggesting that the unique carboxy-terminal domain of TAO2β is required for the endocytosis of the arcadlin protocadherin.

A TAO2β-p38 MAPK Feed-Back Loop Mediates the Endocytosis of Arcadlin

We next investigated the requirement of p38 MAPK for the endocytosis of arcadlin. We found that SB203580, a p38 MAPK inhibitor, blocked the endocytosis of arcadlin (Figure 5G, compare lanes 2 and 3). This suggested that a feed-back loop, in which p38 MAPK regulates the endocytosis of arcadlin, might exist. We first postulated that arcadlin itself was a direct substrate of p38 MAPK. However, arcadlin was not phosphorylated by p38 MAPK (data not shown). We then tested whether p38 MAPK phosphorylates TAO2β. Because the experiments above indicated that the function of TAO2β responsible for the endocytosis of arcadlin resided in the carboxy-terminal domain, the unique carboxy-terminal region (751–1056) of TAO2β was fused to glutathione S-transferase (GST) and subjected to an in vitro kinase reaction with purified p38 MAPK. GST-TAO2β (751–1056) was indeed phosphorylated by activated p38 MAPK (Figure 6A, lane 2). Within this region, there were two sites encoding a serine preceded by a proline in positions 951 and 1010 as possible substrate sites for MAPK family members (Figure 6B; Kyriakis and Avruch, 2001), but their mutation into phosphorylation-resistant alanines did not affect the incorporation of ^{32}P (Figure 6A, lane 3 and data not shown). A detailed deletion mutant analysis (data not shown) then revealed that the main target of p38 MAPK was localized within the region between positions 1036 and 1056 (Figure 6B). We generated Ser to Ala point mutations on positions 1038, 1040, 1042, and 1045 and found that incorporation of ^{32}P diminished in TAO2βS1038A, indicating that Ser1038 is the main target of p38 MAPK (Figures 6A and 6B, lane 4).

We next investigated whether phosphorylation of Ser1038 was required for the endocytosis of arcadlin. Cells expressing TAO2βS951A, used here as a control, exhibited normal endocytosis of arcadlin, whereas the phosphorylation-resistant TAO2βS1038A remained in the surface after addition of Acad-EC protein (Figure 6C, lanes 1–4; see Figure 6D for quantification). Time-lapse images of HEK293T cells expressing arcadlin-EYFP and TAO2βS1038A-ECFP or control TAO2βS951A-ECFP confirmed that TAO2βS1038A fails to induce the endocytosis of arcadlin in living cells (Figure 6E).

These results indicate that the p38 MAPK that is activated by the arcadlin-TAO2β-MEK3 signaling pathway in turn phosphorylates TAO2β on Ser1038, resulting in the formation of a feed-back signaling loop. Phosphorylation of Ser1038 of TAO2β seems to be essential to activate the endocytic machinery following homophilic interaction of arcadlin. Thus, it appears we have identified a molecular pathway for protocadherin-mediated endocytosis.

The Arcadlin-TAO2β-p38 MAPK Pathway Regulates N-Cadherin Endocytosis

Finally, we tested whether the arcadlin-induced internalization of N-cadherin is mediated by the arcadlin-TAO2β-p38 MAPK molecular pathway defined above. The quantification of neuronal surface proteins by biotinylation showed that treatment with Acad-EC caused the reduction in surface arcadlin/N-cadherin levels in neurons (Figure 7A; see Figure 7B for quantification). This reduction was inhibited by SB203580, suggesting that the internalization was mediated by the p38 MAPK pathway (Figures 7A and 7B). Although arcadlin also binds to cadherin-11 (see Figure 1K), there was no significant endocytosis of cadherin-11 upon the treatment with Acad-EC (Figures 7C and 7D). It seems that arcadlin is targeted to multiple species of classical cadherins, but not all of them undergo the endocytosis through this pathway. Individual classical cadherins might code for distinct subsets of synapses.

Similar results were obtained in the microscopic quantification of N-cadherin internalization. A 28.3% ± 2.7% decrease in the mean intensity of total surface N-cadherin in the Acad-EC treatment group (30 min) relative to control was observed. The decrease in the surface N-cadherin mean intensity was observed in both the synaptic and extrasynaptic populations (Figure 7E). In $acad^{-/-}$ neurons, there was no significant change in the mean intensity of total surface N-cadherin in the Acad-EC treatment group relative to control (Figure 7E).

In HEK293T cells cotransfected with *arcadlin*, *N-cadherin*, and *tao2β*, addition of Acad-EC protein also triggered endocytosis (Figure S3). Arcadlin and N-cadherin were cointernalized in the presence of TAO2β but were retained on the plasma membrane in its absence (Figure S3). Taken together, these data indicate that the internalization of N-cadherin is mediated by the arcadlin-TAO2β-p38 MAPK molecular pathway and triggered by homophilic interactions between arcadlin protocadherin extracellular domains.

Arcadlin Mutation Increases Dendritic Spine Density

What is the consequence of the arcadlin-induced internalization of N-cadherin in the dendritic spine membrane? To address this question, we examined the morphology and the number of spines of hippocampal neurons. Cultured hippocampal neurons derived from $acad^{-/-}$ mice protruded a significantly larger number of spines than wild-type neurons (Figure 8B). This phenotype was rescued by the transfection of *arcadlin* cDNA (Figures 8A and 8B and Figure S4A). The rescuing effect was more prominent where the axons of transfected neurons were attached to the transfected dendrites (Figure 8A, square bracket). The other splice variant *arcadlin-L* did not recover the spine

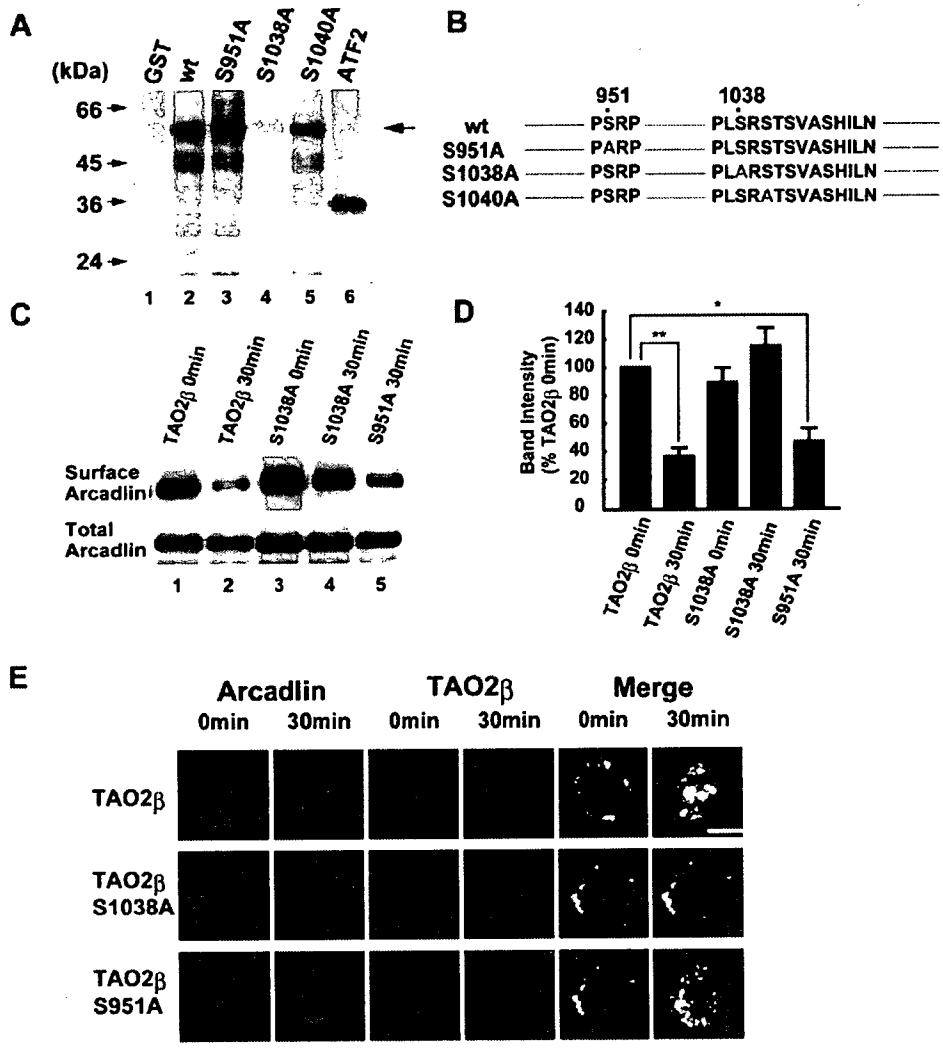

Figure 6. Feed-Back Phosphorylation of TAO2β at Ser1038 by p38 MAPK Is Essential for the Endocytosis of Arcadlin

(A) GST-TAO2β, -TAO2βS951A, -TAO2βS1038A, or -TAO2βS1040A were incubated with activated p38 MAPK and [γ-^{32}P]ATP and subjected to SDS-PAGE followed by autoradiography. The activated p38 MAPK was prepared by immunoprecipitation from Acad-EC-treated HEK293T cells transfected with *arcadlin*, *tao2β*, *MEK3*, and *p38 MAPK*. Arrow indicates ^{32}P-incorporated GST-TAO2β mutant proteins. ATF2, a positive control.

(B) Mutations of TAO2β examined as substrates of p38 MAPK.

(C) Surface-biotinylation assay of arcadlin in HEK293T cells transfected with *arcadlin*, *MEK3*, *p38 MAPK*, and *tao2β* (or *tao2βS1038A* or *tao2βS951A*) before and 30 min after the addition of Acad-EC into culture medium.

(D) Quantification histogram of three independent results of (C) (mean ± SEM).

(E) Time-lapse confocal images of live cells expressing arcadlin-EYFP and TAO2β-ECFP (top), phosphorylation-resistant TAO2βS1038A-ECFP (middle), or control TAO2βS951A-ECFP (bottom) before and 30 min after Acad-EC treatment.

*$p < 0.05$, **$p < 0.01$. Scale bar, 10 μm.

number (Figures 8A and 8B and Figure S4A), indicating that only arcadlin, not arcadlin-L, regulates spine density.

We then asked whether the N-cadherin endocytosis caused the arcadlin-induced change in spine density. There are several studies showing the relationship between N-cadherin activity and spine number. The spine number of *N-cadherin* KO neurons is maintained (Jungling et al., 2006; Kadowaki et al., 2007); a sustained period of N-cadherin loss in these neurons might allow other synaptic cell adhesion molecules to compensate for N-cadherin. In contrast, spine number is suppressed in neurons whose N-cadherin is knocked down by RNAi techniques (Saglietti et al., 2007). Consistently, an expression of a dominant-negative form of N-cadherin reduces the number of synaptic puncta (Togashi et al., 2002). In the present study, the spine density of *acad*$^{-/-}$ neurons was reduced by siRNA knockdown of N-cadherin (Figures 8C and 8D and Figure S4B). Moreover, a similar

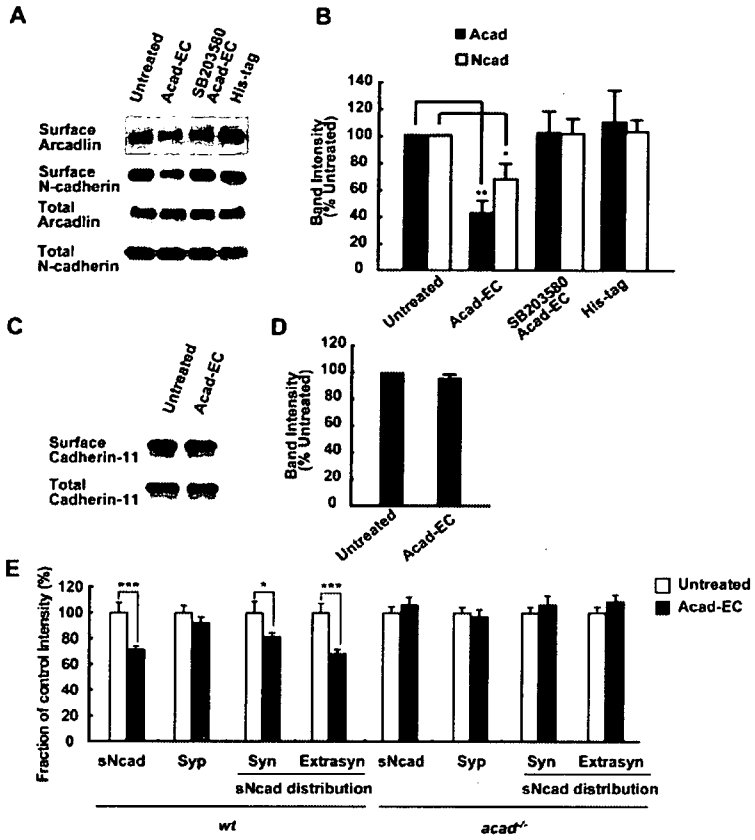

Figure 7. The Arcadlin-TAO2β-p38 MAPK Pathway Mediates the Internalization of N-Cadherin

(A) Internalization of N-cadherin upon treatment of hippocampal neurons with Acad-EC analyzed by labeling surface proteins with biotin. His-tag peptide used as a control.

(B) Quantification of six independent experiments (A) (mean ± SEM).

(C) Surface (top) and total (bottom) cadherin-11 levels in hippocampal neurons with or without Acad-EC treatment were analyzed by immunoblot following the surface labeling with biotin.

(D) Quantification of five independent experiments (C) (mean ± SEM).

(E) Live neurons were incubated with or without Acad-EC prior to the surface N-cadherin labeling. Treatment of neurons with Acad-EC for 30 min resulted in a significant decrease in the surface N-cadherin mean intensity (mean ± SEM) in both the synaptophysin-overlapping fraction (Syn) and synaptophysin-nonoverlapping fraction (Extrasyn) populations. Note that the surface N-cadherin intensity of *acad/papc*$^{-/-}$ neurons did not change. n = 40–50 dendrites from 4–5 independent experiments. $^{*}p < 0.05$, $^{**}p < 0.01$, $^{***}p < 0.001$.

effect was observed by the expression of a dominant-negative form of N-cadherin (NcadΔE) (Figures 8C and 8D). The data suggest that the arcadlin-induced change in spine number is due at least in part to the N-cadherin endocytosis.

DISCUSSION

Our results are consistent with a molecular pathway in which N-cadherin endocytosis is regulated in dendrites by the following sequence of events. (1) Neural activity increases expression of the protocadherin arcadlin in excitatory synapses. (2) Homophilic interactions between extracellular domains of arcadlin molecules activate the phosphorylation of the catalytic domain of the MAPKKK TAO2β, which is constitutively bound to the arcadlin intracellular domain. (3) TAO2β activates p38 MAPK via the MEK3 MAPKK. (4) Activated p38 MAPK feeds-back on TAO2β, phosphorylating it at Ser1038 of its specialized carboxy-terminal regulatory domain. (5) Phosphorylated TAO2β bound to arcadlin initiates the endocytosis of both arcadlin and N-cadherin. The striking effects of mutated or overexpressed arcadlin suggests an *inhibitory* role in regulating the activity of N-cadherin, one of the key molecules involved in spine remodeling (Okamura et al., 2004; Togashi et al., 2002). We propose that this pathway may provide a molecular explanation for how cell-adhesion molecules may transduce synaptic activity into changes in the morphology of dendritic spine membranes (Figure 8E).

Arcadlin Is an Upstream Receptor that Activates the p38 MAPK Pathway

Arcadlin is a member of protocadherin superfamily of cell-adhesion proteins characterized by ~110 amino acid extracellular repeats that possess homophilic binding affinity. Indeed, homophilic cell-adhesion activity of arcadlin/PAPC has been demonstrated (Kim et al., 1998; Yamagata et al., 1999). Our present data also suggests that arcadlin is not a static adhesion protein, but rather plays a highly dynamic role during the remodeling of synaptic spine membrane. Homophilic interactions in *trans* between arcadlin extracellular domains trigger a newly discovered signal transduction cascade connected to p38 MAPK.

The p38 MAPK pathway has been studied extensively (Johnson and Lapadat, 2002). Only recently have neural roles for p38 MAPK in synaptic plasticity been demonstrated (Thomas and Huganir, 2004). To our knowledge, however, there is only one molecule identified as a p38 MAPK regulator in neurons: dual leucine zipper-bearing kinase (DLK), which is a serine/threonine kinase activated by calcium entry at synaptic terminals (Mata et al., 1996). We have now identified TAO2β as another regulator of p38 MAPK in neural tissue. TAO2β is a signal transducer

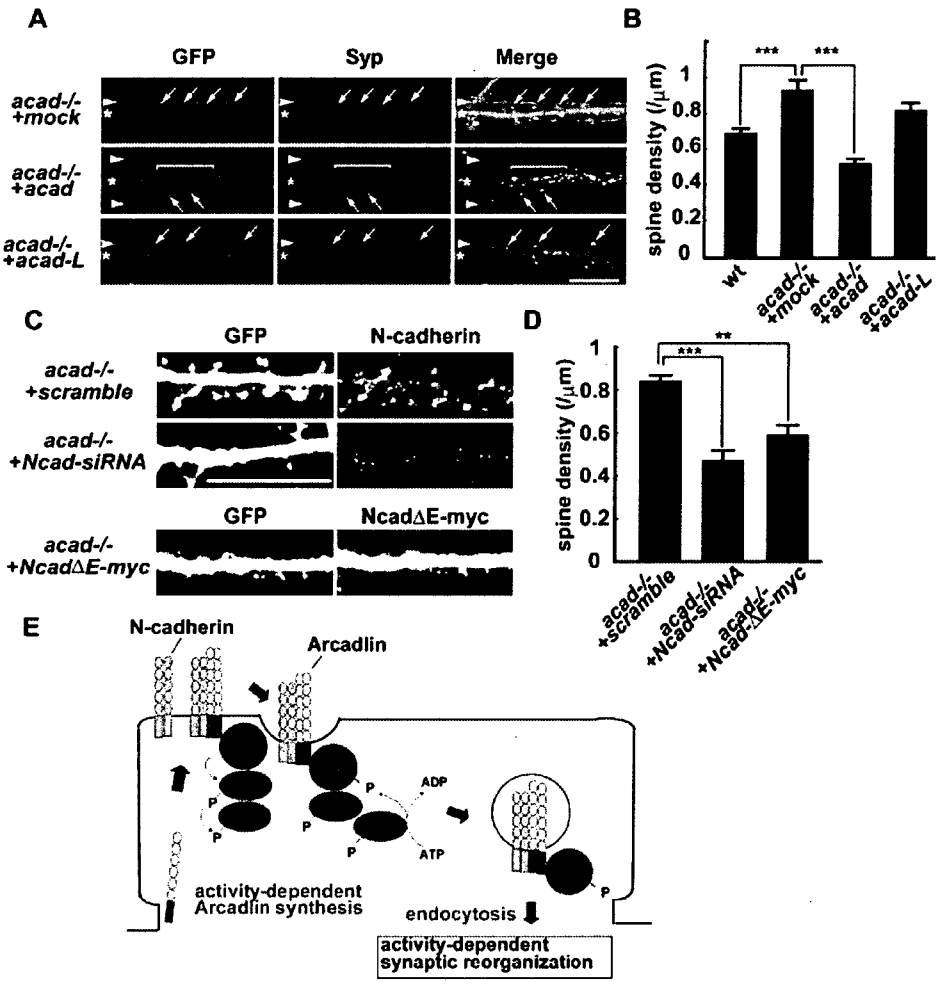

Figure 8. The Effects of Arcadlin on Dendritic Spine Density

(A) Cultured *acad*$^{-/-}$ neurons were doubly transfected with *EGFP* and *mock*, *arcadlin*, or *arcadlin-L* at 6 DIV and visualized with EGFP at 15 DIV. The expressions of arcadlin and arcadlin-L were confirmed by immunocytochemistry (Figure S4A). Arrowheads, axons; asterisks, dendrites; arrows, spine heads attached to axons.

(B) Quantification of dendritic spine density (mean ± SEM) of WT and *acad*$^{-/-}$ neurons transfected with *mock*, *arcadlin*, or *arcadlin-L*. n = 30 independent neurons from 10 independent experiments.

(C) Cultured *acad*$^{-/-}$ neurons were doubly transfected with *EGFP* and *N-cadherin-siRNA (Ncad-siRNA)*, *scramble-siRNA*, or *NcadΔE-myc* at 6 DIV and visualized with GFP at 15 DIV. Expression of N-cadherin was examined by immunocytochemistry. Coexpression of NcadΔE was confirmed by immunostaining for the myc-epitope. The suppression of N-cadherin protein level with the *N-cadherin-siRNA* was confirmed in mouse *N-cadherin-GFP*-transfected HEK293T cells (Figure S4B).

(D) Quantification of dendritic spine density (mean ± SEM) of neurons transfected with *siRNAs* or *NcadΔE*. n = 30 independent neurons from 10 independent experiments.

(E) A model for arcadlin-TAO2β-p38-mediated endocytosis of N-cadherin.

$^{**}p < 0.01$, $^{***}p < 0.001$. Scale bars, 10 μm.

poised close to the inner plasma membrane via association with the intracellular domain of the arcadlin protocadherin. In this sense, the arcadlin protocadherin serves as receptor, rather than an adhesion protein. The observation that the expression of arcadlin is induced after a few hours of synaptic stimulation (Yamagata et al., 1999) suggests that arcadlin serves as a receptor for a late-onset signal transduction pathway resulting in p38 MAPK activation.

The Cytoplasmic Region of Arcadlin Confers Specificity on Signal Transduction

A multitude of protocadherins are expressed in mammalian brain (Wu and Maniatis, 1999). Rat *arcadlin* is the ortholog of human and mouse *pcdh8*, as well as *Xenopus* and zebrafish *papc*. The *arcadlin* cDNA, however, lacks a 294 base pair exon encoding the cytoplasmic region of *pcdh8/papc*, resulting in its gene product having a uniquely short cytoplasmic region (Yamagata et al.,

1999). The long and short forms of arcadlin/PAPC/pcdh8 are differentially expressed in early embryos, implying distinct functions of these isoforms (Makarenkova et al., 2005). The signal transduction pathway transduced by the short form of arcadlin was found here to involve TAO2β, p38 MAPK, and endocytosis. This pathway appears to depend on the shorter cytoplasmic tail of arcadlin, as our unpublished results indicate that the long form of rat arcadlin/PAPC/pcdh8 does not induce p38 MAPK activation or endocytosis.

Endocytosis of Synaptic Cadherin May Lead to the Disruption of Synaptic Adherens Junction

Studies during the past several years have revealed the importance of intracellular trafficking as a means of regulating the functions of classical cadherins (Bryant and Stow, 2004; Chen and Gumbiner, 2006). In epithelial tissues, E-cadherin is a key cell-cell adhesion molecule at adherens junctions and undergoes endocytosis when adherens junctions are disrupted by the action of extracellular signals (Troyanovsky et al., 2006). The dynamin-dependent endocytosis of synaptic N-cadherin triggered by arcadlin may also lead to the disruption of synaptic adherens junctions.

Puncta adherentia are synaptic adherens junctions that reside in the periphery of the synaptic active zone (Uchida et al., 1996). Because the expression of N-cadherin in mature excitatory synapses in hippocampal neurons is concentrated in puncta adherentia, the arcadlin-mediated endocytosis is likely to take place in their vicinity. In fact, the arcadlin immunoreactivity was often found in puncta adherentia in MECS-treated brains (unpublished data). The perisynaptic zone that includes puncta adherentia has recently been recognized as a hot spot of membrane remodeling during synaptic plasticity. AMPA glutamate receptors, for example, undergo activity-dependent delivery to (Shi et al., 1999) and removal from (Zhu et al., 2002) perisynaptic membranes. Synaptic activity-induced activation of the arcadlin-TAO2β-MEK3-p38 signaling pathway could regulate the adhesiveness of synaptic membrane at puncta adherentia and also the activity of neurotransmitter receptors.

Arcadlin-Triggered N-Cadherin Endocytosis Is a Late-Onset Event

Recently, Tai et al. (2007) reported that N-cadherin internalization is surprisingly high under the unstimulated conditions (about 50% of the surface N-cadherin is internalized after 100 min). They have shown that N-cadherin endocytosis is reduced by activating NMDA receptor, and the surface-localized N-cadherins in spines are stabilized with the recruitment of β-catenin into spines. This phenomenon is consistent with the stabilization of surface N-cadherin in response to NMDAR stimulation, as demonstrated by an enhanced resistance to trypsin (Tanaka et al., 2000). Such an enhanced adhesivity of the synaptic membranes, which occurs within a few minutes after the synaptic stimulation, does not require protein synthesis, providing a possible explanation for the short-term remodeling of spine structure (Okamura et al., 2004). On the other hand, the arcadlin-mediated N-cadherin internalization does not operate during these early stages after synaptic stimulation, because the arcadlin-induced internalization of N-cadherin begins at least 4 hr after the stimulation and requires protein synthesis (Figures 1 and 3). Whether or not these arcadlin-dependent and -independent mechanisms share a common endocytic pathway remains to be investigated. Thus, the arcadlin-mediated N-cadherin endocytosis is a late-onset event during the recovery phase following the synaptic stimulation and may provide a homeostatic mechanism balancing total tone and complexity of the neural network.

There is another processing system in which a physiological concentration of glutamate induces a rapid cleavage of N-cadherin (becomes obvious within 15 min) by presenilin-1/γ-secretase, resulting in the generation of cytoplasmic fragment (CTF2) (Marambaud et al., 2003; Uemura et al., 2006). We have confirmed the existence of a 35 kD CTF2 (4.3% ± 1.5% of full-length N-cadherin, n = 5), which increased to 15.6% ± 2.3% (n = 5) after treating with KCl (data not shown). Our experiments showed that the CTF2 amount was not significantly different between 2 and 4 hr after KCl treatment, suggesting that the CTF2 production was completed within 2 hr after neuronal stimulation. On the other hand, our present finding of full-length N-cadherin internalization became evident only after the arcadlin induction at least 4 hr after the stimulation, and occupied as much as 33.8% ± 1.7% of surface N-cadherin (Figure 3B). The internalization of N-cadherin, therefore, is distinct from the presenilin-1/γ-secretase pathway. These two different systems might operate sequentially to regulate surface N-cadherin amount during the activity-dependent processes.

Inhibitory Role of Arcadlin in Dendritic Spine Number

Activity-induced changes in synaptic morphology, including the enlargement of synaptic apposition zones and the emergence of new synapses, have been correlated with long-term potentiation (LTP) (Colicos et al., 2001; Muller et al., 2000; Nagerl et al., 2004). Conversely, long-term depression has been correlated with the pruning of synaptic spines (Nagerl et al., 2004; Zhou et al., 2004). We first thought that arcadlin would be a "positive" regulator of synaptic remodeling, because arcadlin accumulates at the synaptic junction where LTP takes place, and neutralizing antibodies indicated that it is required for the establishment of electrophysiological LTP (Yamagata et al., 1999). Unexpectedly, however, arcadlin loss of function caused an increase in the number of synaptic spines (Figure 8). We observed that the arcadlin neutralizing antibody triggered internalization of surface arcadlin, suggesting that the antibody treatment might block LTP by accelerating the cointernalization with N-cadherin. In addition, it has been shown that other neural activity-regulated molecules, such as MEF2 and SNK, suppress the number of

spines (Flavell et al., 2006; Pak and Sheng, 2003). Our findings suggest that activity-inducible proteins may dampen synaptic function after elevated activity by negatively regulating the spine numbers. In the future, it will be interesting to investigate how arcadlin protocadherin mutations affect learning and memory in the mouse.

In conclusion, the signaling pathway presented here implicates the adhesive apparatus of synaptic spine membranes as a focal point of vigorous synaptic activity-dependent remodeling. The arcadlin-TAO2β-p38 pathway of activity-regulated endocytosis may provide a possible relationship between the modulation of the N-cadherin adhesive machinery and the insertion and removal of neurotransmitter receptors.

EXPERIMENTAL PROCEDURES

Molecular Cloning and Constructing Plasmids

Expression vectors and other plasmids were constructed as described in Supplemental Data. Yeast two-hybrid screening was performed as described previously (Irie et al., 2000). In summary, rat hippocampal cDNAs were subcloned in the SalI/NotI sites of the pPC86 vector, which contains the GAL4 activation domain, and the cytoplasmic region of *arcadlin* was subcloned in-frame in the SalI/NotI sites of the pPC97 vector, which contains the GAL4 DNA binding domain. The plasmids were used to transform PCY2 cells, and positive clones were selected on double-minus plates (Leu−, Trp−) and assayed for β-galactosidase activity.

Cell Culture and Transfection

Details of culture and transfection of COS7, HEK293T cells, and hippocampal neurons from rats (E18) and mice (P0) are provided as Supplemental Data. Inhibition of N-cadherin expression by siRNA was performed as described (Paik et al., 2004). The siRNAs were N-cadherin siRNA (UGUCAAUGGGGUUCUCCACdTdT and GUGGAGAACCCC AUUGACAdTdT) and scrambled siRNA (CAUGCGGAUUCGGAUUU UCdTdT and GAAAAUCCGAAUCCGCAUGdTdT). Oligonucleotides were synthesized by Dharmacon Research Inc., deprotected, and duplexed as described. The target sequence was common for mouse and rat N-cadherin, and their suppression was confirmed in mouse and rat neurons by immunostaining.

Cell-Aggregation Assay

Cell-aggregation assay was performed as described (Takeichi, 1977). Briefly, single cells were prepared by harvesting from monolayer cells with 0.01% crystalline trypsin (type I, Sigma) in HCMF (HEPES-buffered Ca^{2+}- and Mg^{2+}-free HBSS) containing 0.1 mM $CaCl_2$ for 15 min at 37°C followed by supplementation with 0.01% soybean trypsin inhibitor (type I-S, Sigma). 1 × 10^6 cells suspended in 3 ml HCMF were put into each well (2.8 cm × 1.5 cm) and incubated at 37°C on a gyratory shaker at 80 rpm. The total particle number in cell suspension at each time point was counted with a Coulter counter with 100 μm aperture.

Immunostaining

Rat brain sections, cultured hippocampal neurons, and HEK293T cells were fixed with methanol or 2% paraformaldehyde, blocked, and permeabilized with BL solution (5% normal goat serum, 0.1% Triton X-100, 0.02% sodium azide in PBS), and incubated overnight at 4°C with primary antibodies: anti-arcadlin (rabbit, 1:200; Yamagata et al., 1999), anti-N-cadherin (rabbit, 1:200; Okamura et al., 2004; Transduction lab, mouse, 12.5 μg/ml), anti-synaptophysin (Zymed, rabbit, 1:40), anti-PSD-95 (Upstate biotech, mouse, 1:200), anti-GAD6 (Developmental Studies Hybridoma Bank, mouse, 1 μg/ml), anti-NMDA receptor (NR1) (PharMingen, mouse, 1:500), anti-phospho-p38 MAPK (Sigma, mouse, 1:200), anti-GFP (Molecular Probe, rabbit, 1:400), anti-myc (Calbiochem, mouse, 2 μg/ml; Upstate biotech, rabbit, 1:1000), and anti-FLAG (M2) (Sigma, mouse, 1:200). Immunoreactivity was visualized using species-specific fluorochrome-conjugated secondary antibodies.

Immunoprecipitation

Rat hippocampi, cultured neurons, COS7 cells, and HEK293T cells were homogenized with lysis buffers optimized for each tissue and centrifuged to obtain clear protein extracts. The samples were incubated overnight at 4°C with packed 10 μl of protein A Sepharose (GE Healthcare) and specific antibodies: anti-arcadlin (rabbit, 5 μl), anti-TAO2β (rabbit, 5 μl), anti-N-cadherin (Sigma, rabbit, 10 μl), anti-myc (Calbiochem, mouse, 2 μg), and anti-GFP (Molecular Probe, rabbit, 2 μl). The precipitated immune complex was eluted with SDS sample buffer and immunoblotted with specific antibodies: anti-arcadlin (rabbit, 1:2000), anti-TAO2β (rabbit, 1:2000), anti-N-cadherin (Transduction lab, mouse, 1:3000), anti-cadherin-11 (Zymed, mouse, 1:800), anti-β-catenin (Zymed, rabbit, 1:1000), anti-α-catenin (Transduction lab, mouse, 1:250), anti-p120 (Transduction lab, mouse, 1:1000), anti-plakoglobin (Transduction lab, mouse, 1:2000), and anti-myc (Calbiochem, mouse, 1:1000). Details of immunoprecipitation are provided as Supplemental Data.

Characterization of the Association Modes of Arcadlin and N-Cadherin

Association modes of arcadlin-arcadlin and N-cadherin-arcadlin interactions were determined by cell-mix coimmunoprecipitation experiments (Nuriya and Huganir, 2006). The mixture of cells was prepared by transfecting *arcadlin-EGFP* and *arcadlin-flag* (or *N-cadherin*) into two separate dishes of cells, which were once harvested by trypsinization after 24–30 hr and then mixed together in a new dish to allow these two discrete populations of cells to grow in contact with each other. Other groups of cells that were cotransfected with *arcadlin-EGFP* and *arcadlin-flag* (or *N-cadherin*) were treated in the same way. 48 to 50 hr after the transfection, Acad-EC was added to *arcadlin-flag*-expressing cells for 30 min to dissociate the arcadlin-arcadlin interaction. Then, the cells were harvested and subjected to coimmunoprecipitation analyses.

In Vitro Kinase Assay

Activated p38 MAPK was prepared in HEK293T cells transfected with *arcadlin*, *tao2β*, *MEK3*, and *p38 MAPK*. After 48 hr of transfection, cells were exposed to Acad-EC for 30 min and lysed in lysis buffer (20 mM Tris-HCl [pH 7.5], 150 mM NaCl, 1 mM EDTA, 1 mM EGTA, 1% Triton X-100, 2.5 mM sodium pyrophosphate, 1 mM β-glycerophosphate, 1 mM sodium orthovanadate, 1 mg/ml leupeptin, 1 mM PMSF). Cell lysates were incubated with immobilized phospho-p38 MAPK monoclonal antibody (Cell Signaling Technology). To examine which amino acid residue of TAO2β can be phosphorylated by p38 MAPK, substrate (GST-TAO2β751-1056, -TAO2βS951A, -TAO2βS1038A, -TAO2βS1040A, or ATF2) was incubated with immobilized phospho-p38 MAPK in kinase buffer (25 mM Tris-HCl [pH 7.5], 5 mM β-glycerophosphate, 2 mM dithiothreitol, 0.1 mM sodium orthovanadate, 10 mM magnesium chloride) containing 100 μM [γ-^{32}P]ATP at 30°C for 30 min. The phosphorylated proteins were resolved by SDS-PAGE and analyzed by autoradiography.

Surface Biotinylation Assay

After various treatments and washing twice with ice-cold PBS, HEK293T cells and neurons were incubated with EZ-Link Sulfo-NHS-SS-Biotin for 30 min at 4°C. The biotinylation reaction was terminated with three washes with cold TBS. Cells were lysed with RIPA buffer (20 mM Tris-HCl [pH 8.0], 150 mM NaCl, 1 mM EDTA, 1% NP-40, 0.5% deoxycholate, 0.1% SDS, 10 μg/ml leupeptin, 10 μg/ml pepstatin A, 10 μg/ml antipain, 1 mM PMSF) and centrifuged at

10,000 × g at 4°C for 2 min. Immobilized NeutrAvidin Gel (Pierce) was added to the supernatants and incubated at 4°C for 3 hr. After being washed with RIPA buffer, the bound biotinylated proteins were subjected to SDS-PAGE followed by western blot with anti-N-cadherin (Transduction lab, mouse, 1:3000), anti-arcadlin (1:1000), or anti-neuroligin (Synaptic systems, mouse, 1:1000) antibodies. The densitometrically quantified data were statistically analyzed by unpaired two-tailed Student's t test.

Surface N-Cadherin Labeling

Surface N-cadherin labeling was performed as described (Tai et al., 2007) with modifications. Neurons (14–17 DIV) after various treatments were incubated for 30 min on ice in the presence of N-cadherin surface antibody (MT79, 42 μg/ml in ice-cold conditioned medium supplied with 10 mM HEPES-NaOH [pH7.4]). Neurons were rinsed three times with ice-cold HBSS, fixed with 4% paraformaldehyde for 30 min, rinsed three times with PBS, and then incubated with a secondary antibody for 1 hr at RT. After rinsing with PBS and permeabilization with BL, neurons were incubated with primary and secondary antibodies against the intracellular proteins sequentially for 1 hr each at RT. After wash with PBS, neurons were mounted for imaging. Surface N-cadherin staining was imaged with a Zeiss 510 Meta confocal microscope with a 40× objective (NA = 1.3). Each stack was maximal Z-projected into a single stack. Individual neuron within each projected image was registered by using the RegisterROI plug-in of ImageJ software (W. Rasband, National Institutes of Health, Bethesda, MD; http://rsb.info.nih.gov/ij/). Two dendrites were straightened per cell. Average fluorescence intensities were computed separately for spines and shafts in each dendrite. Total dendritic signals represent the sum of spine and shaft signals. Separation of synaptophysin-overlapping fraction from synaptophysin-nonoverlapping fraction populations was performed with the ColocalizeRGB plug-in of ImageJ. The intensity of the overlapping fraction was normalized with the relative intensity for synaptophysin.

Supplemental Data

The Supplemental Data for this article can be found online at http://www.neuron.org/cgi/content/full/56/3/456/DC1/.

ACKNOWLEDGMENTS

We thank Naomasa Miki, Takahiro Fujimoto, and Kirsten Arndt for valuable discussions; Masumi Ichikawa and Junko Kuroda-Kimura for confocal microscopy; Hideru Togashi for advice with culturing mouse neurons; Machiko Kamimoto, Tomoyuki Sugimoto, and Takehisa Uchiyama for statistics; Greg Phillips, Weisong Shan, and David Colman for reagents; Kyoko Suzuki, Hong Shi, and Atsunori Ohnishi for technical assistance. This work was supported by KAKENHIs (12053278, 15300130, and 18209037 to K.Y.; 13210093, 14017063, and 17500253 to H.T.) Y.Y. is supported by National Institute of Health (NS20147). E.M.D.R. is an Investigator of the Howard Hughes Medical Institute.

Received: February 15, 2007
Revised: June 15, 2007
Accepted: August 27, 2007
Published: November 7, 2007

REFERENCES

Bailey, C.H., Chen, M., Keller, F., and Kandel, E.R. (1992). Serotonin-mediated endocytosis of apCAM: an early step of learning-related synaptic growth in Aplysia. Science *256*, 645–649.

Benson, D.L., and Tanaka, H. (1998). N-cadherin redistribution during synaptogenesis in hippocampal neurons. J. Neurosci. *18*, 6892–6904.

Bozdagi, O., Shan, W., Tanaka, H., Benson, D.L., and Huntley, G.W. (2000). Increasing numbers of synaptic puncta during late-phase LTP: N-cadherin is synthesized, recruited to synaptic sites, and required for potentiation. Neuron *28*, 245–259.

Bryant, D.M., and Stow, J.L. (2004). The ins and outs of E-cadherin trafficking. Trends Cell Biol. *14*, 427–434.

Chen, X., and Gumbiner, B.M. (2006). Paraxial protocadherin mediates cell sorting and tissue morphogenesis by regulating C-cadherin adhesion activity. J. Cell Biol. *174*, 301–313.

Chen, Z., Hutchison, M., and Cobb, M.H. (1999). Isolation of the protein kinase TAO2 and identification of its mitogen-activated protein kinase/extracellular signal-regulated kinase kinase binding domain. J. Biol. Chem. *274*, 28803–28807.

Chen, Z., Raman, M., Chen, L., Lee, S.F., Gilman, A.G., and Cobb, M.H. (2003). TAO (thousand-and-one amino acid) protein kinases mediate signaling from carbachol to p38 mitogen-activated protein kinase and ternary complex factors. J. Biol. Chem. *278*, 22278–22283.

Colicos, M.A., Collins, B.E., Sailor, M.J., and Goda, Y. (2001). Remodeling of synaptic actin induced by photoconductive stimulation. Cell *107*, 605–616.

Cooney, J.R., Hurlburt, J.L., Selig, D.K., Harris, K.M., and Fiala, J.C. (2002). Endosomal compartments serve multiple hippocampal dendritic spines from a widespread rather than a local store of recycling membrane. J. Neurosci. *22*, 2215–2224.

Fannon, A.M., and Colman, D.R. (1996). A model for central synaptic junctional complex formation based on the differential adhesive specificities of the cadherins. Neuron *17*, 423–434.

Flavell, S.W., Cowan, C.W., Kim, T.K., Greer, P.L., Lin, Y., Paradis, S., Griffith, E.C., Hu, L.S., Chen, C., and Greenberg, M.E. (2006). Activity-dependent regulation of MEF2 transcription factors suppresses excitatory synapse number. Science *311*, 1008–1012.

Huber, O., Kemler, R., and Langosch, D. (1999). Mutations affecting transmembrane segment interactions impair adhesiveness of E-cadherin. J. Cell Sci. *112*, 4415–4423.

Irie, Y., Yamagata, K., Gan, Y., Miyamoto, K., Do, E., Kuo, C.H., Taira, E., and Miki, N. (2000). Molecular cloning and characterization of Amida, a novel protein which interacts with a neuron-specific immediate early gene product arc, contains novel nuclear localization signals, and causes cell death in cultured cells. J. Biol. Chem. *275*, 2647–2653.

Johnson, G.L., and Lapadat, R. (2002). Mitogen-activated protein kinase pathways mediated by ERK, JNK, and p38 protein kinases. Science *298*, 1911–1912.

Jungling, K., Eulenburg, V., Moore, R., Kemler, R., Lessmann, V., and Gottmann, K. (2006). N-Cadherin transsynaptically regulates short-term plasticity at glutamatergic synapses in embryonic stem cell-derived neurons. J. Neurosci. *26*, 6968–6978.

Kadowaki, M., Nakamura, S., Machon, O., Krauss, S., Radice, G.L., and Takeichi, M. (2007). N-cadherin mediates cortical organization in the mouse brain. Dev. Biol. *304*, 22–33.

Kamiguchi, H., and Lemmon, V. (2000). Recycling of the cell adhesion molecule L1 in axonal growth cones. J. Neurosci. *20*, 3676–3686.

Kim, S.H., Yamamoto, A., Bouwmeester, T., Agius, E., and De Robertis, E.M. (1998). The role of paraxial protocadherin in selective adhesion and cell movements of the mesoderm during Xenopus gastrulation. Development *125*, 4681–4690.

Kyriakis, J.M., and Avruch, J. (2001). Mammalian mitogen-activated protein kinase signal transduction pathways activated by stress and inflammation. Physiol. Rev. *81*, 807–869.

Makarenkova, H., Sugiura, H., Yamagata, K., and Owens, G. (2005). Alternatively spliced variants of protocadherin 8 exhibit distinct patterns of expression during mouse development. Biochim. Biophys. Acta *1681*, 150–156.

Manabe, T., Togashi, H., Uchida, N., Suzuki, S.C., Hayakawa, Y., Yamamoto, M., Yoda, H., Miyakawa, T., Takeichi, M., and Chisaka, O. (2000). Loss of cadherin-11 adhesion receptor enhances plastic changes in hippocampal synapses and modifies behavioral responses. Mol. Cell. Neurosci. *15*, 534–546.

Marambaud, P., Wen, P.H., Dutt, A., Shioi, J., Takashima, A., Siman, R., and Robakis, N.K. (2003). A CBP binding transcriptional repressor produced by the PS1/[epsilon]-cleavage of N-cadherin is inhibited by PS1 FAD mutations. Cell *114*, 635–645.

Mata, M., Merritt, S.E., Fan, G., Yu, G.G., and Holzman, L.B. (1996). Characterization of dual leucine zipper-bearing kinase, a mixed lineage kinase present in synaptic terminals whose phosphorylation state is regulated by membrane depolarization via calcineurin. J. Biol. Chem. *271*, 16888–16896.

Muller, D., Toni, N., and Buchs, P.A. (2000). Spine changes associated with long-term potentiation. Hippocampus *10*, 596–604.

Murase, S., Mosser, E., and Schuman, E.M. (2002). Depolarization drives beta-Catenin into neuronal spines promoting changes in synaptic structure and function. Neuron *35*, 91–105.

Nagerl, U.V., Eberhorn, N., Cambridge, S.B., and Bonhoeffer, T. (2004). Bidirectional activity-dependent morphological plasticity in hippocampal neurons. Neuron *44*, 759–767.

Nuriya, M., and Huganir, R.L. (2006). Regulation of AMPA receptor trafficking by N-cadherin. J. Neurochem. *97*, 652–661.

Okamura, K., Tanaka, H., Yagita, Y., Saeki, Y., Taguchi, A., Hiraoka, Y., Zeng, L.H., Colman, D.R., and Miki, N. (2004). Cadherin activity is required for activity-induced spine remodeling. J. Cell Biol. *167*, 961–972.

Paik, J.-H., Skoura, A., Chae, S.-S., Cowan, A.E., Han, D.K., Proia, R.L., and Hla, T. (2004). Sphingosine 1-phosphate receptor regulation of N-cadherin mediates vascular stabilization. Genes Dev *18*, 2392–2403.

Pak, D.T.S., and Sheng, M. (2003). Targeted protein degradation and synapse remodeling by an inducible protein kinase. Science *302*, 1368–1373.

Racz, B., Blanpied, T.A., Ehlers, M.D., and Weinberg, R.J. (2004). Lateral organization of endocytic machinery in dendritic spines. Nat. Neurosci. *7*, 917–918.

Saglietti, L., Dequidt, C., Kamieniarz, K., Rousset, M.-C., Valnegri, P., Thoumine, O., Beretta, F., Fagni, L., Choquet, D., Sala, C., et al. (2007). Extracellular interactions between GluR2 and N-cadherin in spine regulation. Neuron *54*, 461–477.

Shi, S.H., Hayashi, Y., Petralia, R.S., Zaman, S.H., Wenthold, R.J., Svoboda, K., and Malinow, R. (1999). Rapid spine delivery and redistribution of AMPA receptors after synaptic NMDA receptor activation. Science *284*, 1811–1816.

Strehl, S., Glatt, K., Liu, Q.M., Glatt, H., and Lalande, M. (1998). Characterization of two novel protocadherins (PCDH8 and PCDH9) localized on human chromosome 13 and mouse chromosome 14. Genomics *53*, 81–89.

Sytnyk, V., Leshchyns'ka, I., Nikonenko, A.G., and Schachner, M. (2006). NCAM promotes assembly and activity-dependent remodeling of the postsynaptic signaling complex. J. Cell Biol. *174*, 1071–1085.

Tai, C.Y., Mysore, S.P., Chiu, C., and Schuman, E.M. (2007). Activity-regulated N-cadherin endocytosis. Neuron *54*, 771–785.

Takeichi, M. (1977). Functional correlation between cell adhesive properties and some cell surface proteins. J. Cell Biol. *75*, 464–474.

Tanaka, H., Shan, W., Phillips, G.R., Arndt, K., Bozdagi, O., Shapiro, L., Huntley, G.W., Benson, D.L., and Colman, D.R. (2000). Molecular modification of N-cadherin in response to synaptic activity. Neuron *25*, 93–107.

Tang, L., Hung, C.P., and Schuman, E.M. (1998). A role for the cadherin family of cell adhesion molecules in hippocampal long-term potentiation. Neuron *20*, 1165–1175.

Thomas, G.M., and Huganir, R.L. (2004). MAPK cascade signalling and synaptic plasticity. Nat. Rev. Neurosci. *5*, 173–183.

Tibbles, L.A., and Woodgett, J.R. (1999). The stress-activated protein kinase pathways. Cell. Mol. Life Sci. *55*, 1230–1254.

Togashi, H., Abe, K., Mizoguchi, A., Takaoka, K., Chisaka, O., and Takeichi, M. (2002). Cadherin regulates dendritic spine morphogenesis. Neuron *35*, 77–89.

Troyanovsky, R.B., Sokolov, E.P., and Troyanovsky, S.M. (2006). Endocytosis of cadherin from intracellular junctions is the driving force for cadherin adhesive dimer disassembly. Mol. Biol. Cell *17*, 3484–3493.

Uchida, N., Honjo, Y., Johnson, K.R., Wheelock, M.J., and Takeichi, M. (1996). The catenin/cadherin adhesion system is localized in synaptic junctions bordering transmitter release zones. J. Cell Biol. *135*, 767–779.

Uemura, K., Kihara, T., Kuzuya, A., Okawa, K., Nishimoto, T., Bito, H., Ninomiya, H., Sugimoto, H., Kinoshita, A., and Shimohama, S. (2006). Activity-dependent regulation of β-catenin via ε-cleavage of N-cadherin. Biochem. Biophys. Res. Commun. *345*, 951–958.

Wu, Q., and Maniatis, T. (1999). A striking organization of a large family of human neural cadherin-like cell adhesion genes. Cell *97*, 779–790.

Yamagata, K., Andreasson, K.I., Sugiura, H., Maru, E., Dominique, M., Irie, Y., Miki, N., Hayashi, Y., Yoshioka, M., Kaneko, K., et al. (1999). Arcadlin is a neural activity-regulated cadherin involved in long term potentiation. J. Biol. Chem. *274*, 19473–19479.

Yamamoto, A., Kemp, C., Bachiller, D., Geissert, D., and De Robertis, E.M. (2000). Mouse paraxial protocadherin is expressed in trunk mesoderm and is not essential for mouse development. Genesis *27*, 49–57.

Zhou, Q., Homma, K.J., and Poo, M.M. (2004). Shrinkage of dendritic spines associated with long-term depression of hippocampal synapses. Neuron *44*, 749–757.

Zhu, J.J., Qin, Y., Zhao, M., Van Aelst, L., and Malinow, R. (2002). Ras and Rap control AMPA receptor trafficking during synaptic plasticity. Cell *110*, 443–455.

Accession Number

We have deposited the sequence for the new isoform of TAO2 kinase (=TAO2β) into DDBJ (http://www.ddbj.nig.ac.jp/). The accession number is AB290408.

European Journal of Neuroscience, Vol. 26, pp. 126–133, 2007 doi:10.1111/j.1460-9568.2007.05640.x

Granulocyte colony-stimulating factor has a negative effect on stroke outcome in a murine model

Akihiko Taguchi,[1] Zhongmin Wen,[1] Kazunori Myojin,[1] Tomoyuki Yoshihara,[1] Takayuki Nakagomi,[2] Daisuke Nakayama,[1] Hidekazu Tanaka,[3] Toshihiro Soma,[4] David M. Stern,[5] Hiroaki Naritomi[1] and Tomohiro Matsuyama[2]

[1]Department of Cerebrovascular Disease, National Cardiovascular Center, 5-7-1 Fujishiro-dai, Suita, Osaka, Japan, 565-8565
[2]Department of Advanced Medicine, Hyogo College of Medicine, Hyogo, Japan
[3]Department of Pharmacology, Graduate School of Medicine, Osaka University, Osaka, Japan
[4]Department of Hematology, Osaka Minami National Hospital, Osaka, Japan
[5]Dean's Office, College of Medicine, University of Cincinnati, OH, USA

Keywords: angiogenesis, cerebral infarction, inflammation, neuroprotection

Abstract

The administration of CD34-positive cells after stroke has been shown to have a beneficial effect on functional recovery by accelerating angiogenesis and neurogenesis in rodent models. Granulocyte colony-stimulating factor (G-CSF) is known to mobilize CD34-positive cells from bone marrow and has displayed neuroprotective properties after transient ischemic stress. This led us to investigate the effects of G-CSF administration after stroke in mouse. We utilized permanent ligation of the M1 distal portion of the left middle cerebral artery to develop a reproducible focal cerebral ischemia model in CB-17 mice. Animals treated with G-CSF displayed cortical atrophy and impaired behavioral function compared with controls. The negative effect of G-CSF on outcome was associated with G-CSF induction of an exaggerated inflammatory response, based on infiltration of the peri-infarction area with CD11b-positive and F4/80-positive cells. Although clinical trials with G-CSF have been started for the treatment of myocardial and limb ischemia, our results indicate that caution should be exercised in applying these results to cerebral ischemia.

Introduction

Granulocyte colony-stimulating factor (G-CSF) was identified in 1975 and has been broadly used for mobilizing granulocytes from bone marrow (Weaver *et al.*, 1993). G-CSF is also known to mobilize immature hematopoietic cells that include endothelial progenitor cells (EPCs) (Willing *et al.*, 2003). In view of the capacity of circulating EPCs to enhance neovascularization of ischemic tissues (Asahara *et al.*, 1997), the results of recent studies demonstrating that infusion of EPCs accelerates angiogenesis at ischemic sites, thereby limiting tissue injury, is not unexpected (Dzau *et al.*, 2005). As a potential extension of this concept, administration of G-CSF has been shown to accelerate angiogenesis in animal models of limb and myocardial ischemia (Minatoguchi *et al.*, 2004). These observations have provided a foundation for clinical trials testing the effects of G-CSF in limb and myocardial ischemia (Kuethe *et al.*, 2004).

Stroke, a critical ischemic disorder in which there are important opportunities for neuroprotective therapies, is another situation in which enhanced angiogenesis might be expected to improve outcome. For example, we have shown that the administration of CD34-positive cells after stroke accelerates angiogenesis and, subsequently, neurogenesis (Taguchi *et al.*, 2004). Similarly, erythropoietin (EPO), also known to have angiogenic properties, has been shown to have beneficial effects in experimental cerebral ischemia (Ehrenreich *et al.*, 2002; Wang *et al.*, 2004). In addition, G-CSF displays neuroprotective properties *in vitro* (Schabitz *et al.*, 2003) and *in vivo* (Schabitz *et al.*, 2003; Shyu *et al.*, 2004; Gibson *et al.*, 2005), the latter in a rodent model of transient cerebral ischemic damage. Models of transient cerebral ischemia allow subtle assessment of neuroprotective properties, such as the survival of vulnerable neuronal populations in the penumbra. However, functional outcome after stroke is also determined by inflammation and reparative processes consequent to extensive brain necrosis, the latter better modelled by permanent cerebral ischemia. We have evaluated the effect of G-CSF on stroke outcome in a model of permanent cerebral ischemia with massive cell necrosis. Our model employs permanent ligation of the left middle cerebral artery (MCA) and results in extensive neuronal death in the ischemic zone, as well as more selective apoptotic cell death in the penumbral area (Walther *et al.*, 2002). Using this model, we have tested the effect of G-CSF on functional recovery after stroke.

Materials and methods

All procedures were performed under the auspices of an approved protocol of the Japanese National Cardiovascular Center Animal Care and Use Committees (protocol no. 06026, approval date, May 22, 2006).

Induction of focal cerebral ischemia

To assess the effect of G-CSF on stroke, we developed a highly reproducible murine stroke model applying our previous method

Correspondence: Dr Akihiko Taguchi, as above.
E-mail: ataguchi@res.ncvc.go.jp

Received 19 October 2006, revised 25 April 2007, accepted 21 May 2007

(Taguchi *et al.*, 2004) to CB-17 mice (Clea, Tokyo, Japan). Under halothane anesthesia (inhalation of 3%), the left zygoma was dissected to visualize the MCA through the cranial bone. A hole was made using a dental drill in the bone (diameter 1.5 mm) and the MCA was carefully isolated, electro-cauterized and disconnected just distal to its crossing of the olfactory tract (distal M1 portion). Cerebral blood flow in the MCA area was monitored as described previously (Matsushita *et al.*, 1998). Briefly, an acrylate column was attached to the intact skull using stereotactic coordinates (1 mm anterior and 3 mm lateral to the bregma) and cerebral blood flow was assessed using a linear probe (1 mm in diameter) by laser Doppler flowmetry (Neuroscience Co. Ltd, Osaka, Japan). Mice that showed decreased cerebral blood flow by ~75% immediately after the procedure were used for experiments (success rate of > 95%). Body temperature was maintained at 36.5–37 °C using a heat lamp (Nipponkoden, Tokyo, Japan) during the operation and for 2 h after MCA occlusion. At later timepoints, mice were first subjected to behavioral tests and then to histological examination of their brains. For histological examination, mice were perfusion-fixed with 100 mL of periodate-lysine-paraformaldehyde fixative under deep (pentobarbital) anesthesia (100 mg/kg, intraperitonealy) and their brains were removed. Coronal brain sections (20 μm) were cut on a vibratome (Leica, Solms, Germany) and subjected to immunocytochemistry.

Administration of granulocyte colony-stimulating factor and erythropoietin following stroke

To examine the effect of G-CSF on ischemic cerebral injury, human recombinant G-CSF (Kirin, Tokyo, Japan) was administered subcutaneously at four doses (0.5, 5, 50 or 250 μg/kg) at 24, 48 and 72 h after induction of stroke. As controls, the same volume of phosphate-buffered saline (PBS) or recombinant human EPO (1000 μg/kg; Kirin), the latter known to have angiogenic properties and a positive effect on stroke outcome (Jaquet *et al.*, 2002), was administered subcutaneously. Other time courses of G-CSF administration, including 1 h after stroke (at doses of 0.5, 5, 50 or 250 μg/kg) and continuous administration (100 μg/kg/day) by micro-osmotic pump (Durect, Cupertino, CA, USA) started 1 h after stroke over 7 days, were also studied. To exclude possible effects of an immune response to human recombinant G-CSF in the mouse, murine recombinant G-CSF (R & D Systems, Minneapolis, MN, USA; doses of 0.5, 5 or 50 μg/kg) was administered subcutaneously at 24, 48 and 72 h after induction of stroke, as indicated.

Immunohistochemistry

To evaluate the inflammatory response following administration of G-CSF post-stroke, brain sections were studied immunohistochemically using antibody to CD11b (BD Biosciences, San Jose, CA, USA) and F4/80 (Serotec, Raleigh, NC, USA). The numbers of CD11b-positive inflammatory cells at the anterior cerebral artery (ACA)/MCA border of the infarcted area and numbers of F4/80-positive ($F4/80^+$) activated microglia/macrophages in the ACA area at the exact center of the forebrain section (at the midpoint of the left forebrain, as shown with an orange line in Fig. 1J) were scored by two investigators blinded to the experimental protocol.

Analysis of the peri-infarction and infarcted area after middle cerebral artery occlusion

To investigate mechanisms of brain damage/atrophy consequent to administration of G-CSF, neovessel formation and the extent of infarction were analysed. Formation of new vessels was assessed at the border of the MCA and ACA territories by perfusing carbon black (0.5 mL; Fuekinori, Osaka, Japan) via the left ventricle of the heart. Staining with 2,3,5-triphenyltetrazolium (TTC) (Sigma-Aldrich, St Louis, MO, USA) was employed to demarcate the border of viable/non-viable tissue. Semiquantitative analysis of angiogenesis employed an angiographic score. Briefly, microscopic digital images were scanned into a computer (Keyence, Osaka, Japan) and the number of carbon black-positive microvessels crossing the border zone of the TTC-negative MCA area to the TTC-positive ACA area was determined. To evaluate the infarcted area 3 days after stroke, coronal brain sections at the exact center of the forebrain were stained with TTC. The infarcted area was measured using a microscopic digital camera system (Olympus, Tokyo, Japan). Infarction in this stroke model was highly reproducible and limited to the left cortex. NIH IMAGE software was used to quantify the TTC-positive area in the ACA territory. A brain atrophy index was established using whole brain images captured by a digital camera system (Olympus). The length of the forebrain was measured along the x and y dimensions shown in Fig. 1J and the ratio of $x : y$ was defined as the brain atrophy index.

Behavioral analysis

To assess cortical function, mice were subjected to behavioral testing using the open field task (Kimble, 1968) at 35 days after stroke. In this behavioral paradigm, animals were allowed to search freely in a square acrylic box (30 × 30 cm) for 60 min. A light source on the ceiling of the enclosure was on during the first 30 min (light period) and was turned off during a subsequent 30-min period. On the X- and Y-banks of the open field, two infrared beams were mounted 2 cm above the floor, spaced at 10 cm intervals, forming a flip–flop circuit between them. The total number of beam crossings by the animal was counted and scored as traveling behavior (locomotion). Twelve infrared beams were set 5 cm above the floor, spaced at 3 cm intervals, on the X-bank and the total number of beam crossings was counted and scored as rearing behavior (rearing). To exclude the contribution of physical deficits directly related to the operative procedure and induction of stroke, motor deficiencies were examined on day 35 after stroke. Neurological deficits were scored on a three-point modified scale as described previously (Tamatani *et al.*, 2001): 0, no neurological deficit; 1, failure to extend the left forepaw fully; 2, circling to left and 3, loss of walking or righting reflex. Body weight, monitored in each experimental group, displayed no significant differences (data not shown).

Data analysis

Statistical comparisons among groups were determined using one-way ANOVA and the Dunnett test was used for post-hoc analysis to compare with PBS controls. Where indicated, individual comparisons were performed using Student's t-test. In all experiments, mean ± SEM is reported.

Results

Induction of stroke in CB-17 mice

In a previous report, we demonstrated reproducible strokes in severe combined immunodeficient (SCID) mice by permanent ligation of the left MCA (Taguchi *et al.*, 2004). As SCID mice originated from the CB-17 strain, we expected anatomical similarity of cerebral arteries in

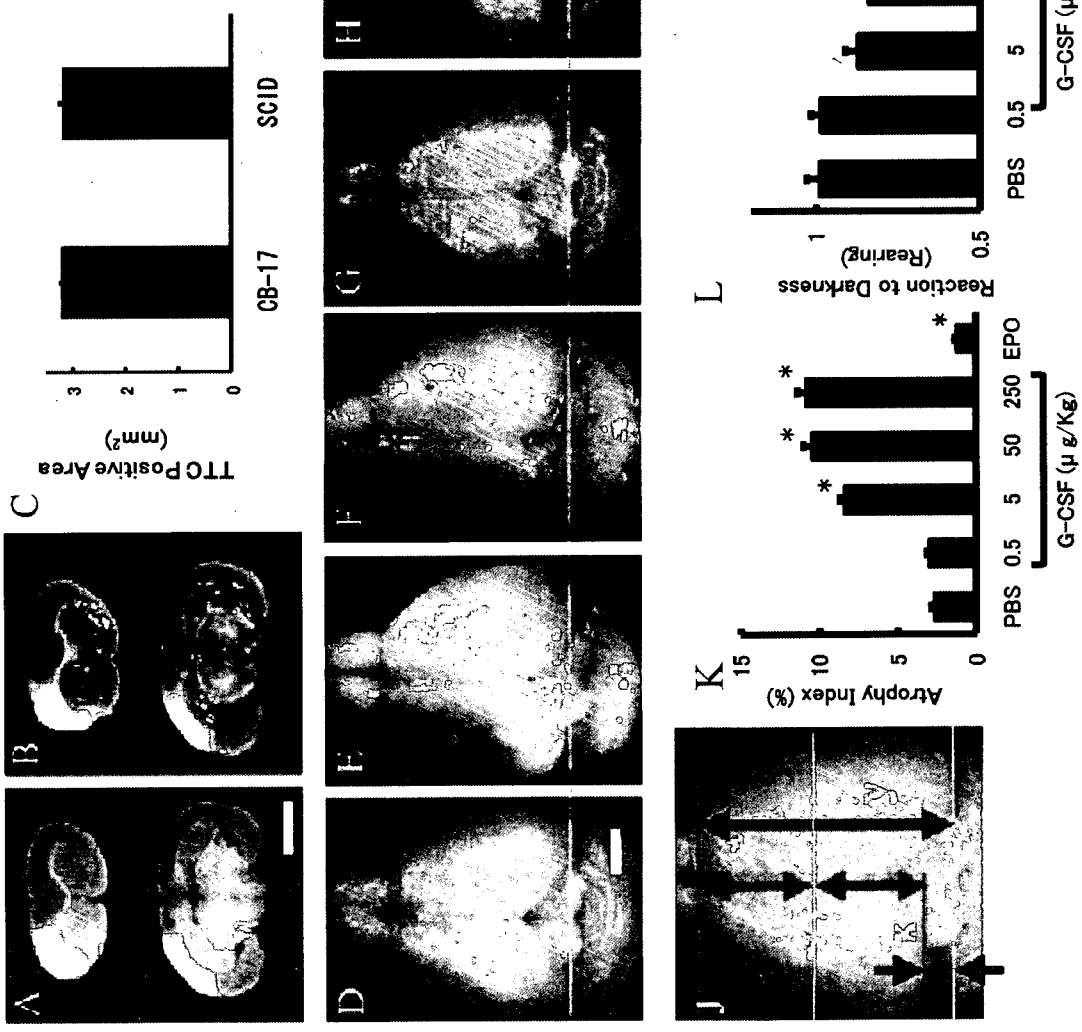

FIG. 1. Administration of granulocyte colony-stimulating factor (G-CSF) induces cortical atrophy. (A–C) Induction of stroke by ligation of the M1 portion of the left middle cerebral artery (MCA). Forebrain sections harvested from mice 3 h after stroke were stained with 2,3,5-triphenyltetrazolium (TTC), and lack of positive staining is observed in the MCA cortex of CB-17 (A) and severe combined immunodeficient (SCID) mice (B). The TTC-positive anterior cerebral artery area at the exact center of forebrain was quantified using NIH IMAGE (C). A highly reproducible TTC-positive (surviving) cortical area was observed in CB-17 and SCID mice. (D–J) On day 35 post-stroke, brains were evaluated grossly. Compared with post-stroke mice treated with phosphate-buffered saline (PBS) (D), no significant difference was observed in mice treated with 0.5 μg/kg of G-CSF (E). In contrast, brain atrophy was observed with G-CSF treatment at doses of 5 μg/kg (F), 50 μg/kg (G) or 250 μg/kg (H). Treatment with erythropoietin (EPO) (I) had a beneficial effect in terms of brain atrophy. Note that, compared with the contralateral side (green line), atrophy in the longitudinal direction was observed in animals treated with G-CSF (F–H). (J) A brain atrophy index was defined as the ratio of $x : y$. (K) ANOVA analysis ($n = 6$ per group) revealed significant brain atrophy in mice at doses of G-CSF above 0.5 μg/kg. In contrast, a reduction of brain atrophy was observed in mice treated with EPO. (L and M) Behavioral analysis post-stroke. ANOVA analysis ($n = 6$ per group) in mice subjected to stroke revealed that treatment with either 50 or 250 μg/kg of G-CSF significantly impaired the rearing response compared with PBS (L), although no significant difference was observed in locomotion (M). Marker bars, 2 mm (A and D). $^*P < 0.05$ vs. PBS.

these two strains. Strokes were induced in CB-17 mice by permanent ligation of the M1 distal portion of the left MCA. To evaluate the infarcted area, brain sections were stained with TTC at 3 h after stroke. Reproducible strokes were induced in CB-17 mice (Fig. 1A) that were similar to those in SCID mice (Fig. 1B). The surviving cortical area post-stroke, represented by the TTC-positive ACA area at the exact center of forebrain, was also similar in CB-17 and SCID mice (Fig. 1C, $n = 6$/species).

Granulocyte colony-stimulating factor accelerates brain injury after stroke

In a previous study, we demonstrated that enhanced neovascularization post-stroke, due to administration of CD34-positive cells, promoted neuronal regeneration leading to cortical expansion and functional recovery (Taguchi *et al.*, 2004). As G-CSF is known to mobilize CD34-positive cells from bone marrow (Kuethe *et al.*, 2004), we investigated the effects of G-CSF treatment, starting 24 h after stroke and continuing for 3 days, using the above permanent focal cerebral ischemia model. Compared with control animals receiving PBS alone (Fig. 1D), no significant difference was observed in mice that received 0.5 μg/kg of G-CSF (Fig. 1E and K) at 35 days after stroke. However, remarkable brain atrophy was observed with G-CSF treatment at 5 μg/kg (Fig. 1F and K), 50 μg/kg (Fig. 1G and K) or 250 μg/kg (Fig. 1H and K). In contrast, a mild protective effect, with respect to brain atrophy, was observed in the group treated with EPO post-stroke (1000 μg/kg; Fig. 1I and K). In each condition depicted in Fig. 1, a representative image is shown and quantitative analysis of the brain atrophy index ($n = 6$/experimental condition; defined in Fig. 1J) is demonstrated in Fig. 1K.

Granulocyte colony-stimulating factor has a negative effect on functional recovery after stroke

To investigate functional recovery in animals treated with G-CSF, we performed behavioral testing on day 35 after stroke ($n = 6$, for each group). Compared with post-stroke CB-17 mice that received PBS, mice treated with 50 or 250 μg/kg G-CSF displayed impaired behavioral function as assessed by the 'dark' response, with respect to rearing (Fig. 1L and Table 1) analysed by ANOVA followed by post-hoc Dunnett test, although there was no significant change in locomotion (Fig. 1M). In contrast, treatment with EPO accelerated functional recovery with respect to both rearing (1.18 ± 0.07 and 0.99 ± 0.04 in EPO and PBS groups, respectively, $n = 6$ per group, $P < 0.05$) and locomotion (1.04 ± 0.04 and 0.85 ± 0.04 in EPO and PBS groups, respectively, $n = 6$ per group, $P < 0.05$). Mice showed rapid recovery from focal motor deficits and, by day 16 post-stroke, no motor deficits were detected based on a modified three-point scale (not shown).

Granulocyte colony-stimulating factor accelerates angiogenesis after stroke

Increased brain atrophy and impaired functional recovery in animals treated with G-CSF post-stroke were quite unexpected because of the known ability of G-CSF to mobilize CD34-positive cells from bone marrow (Willing *et al.*, 2003). In addition, a previous study showed neuroprotective properties of G-CSF in models of transient cerebral ischemia (Schabitz *et al.*, 2003). These considerations led us to analyse mechanisms contributing to increased brain atrophy after

TABLE 1. Raw data of open field test (G-CSF rearing)

Treatment and individual	Rearing (counts)		Reaction to darkness (Right OFF/Right ON)
	Right ON	Right OFF	
PBS			
1	662	640	0.97
2	611	708	1.16
3	487	450	0.92
4	587	540	0.92
5	482	430	0.89
6	425	450	1.06
Mean ± SEM	542.3 ± 37.2	536.3 ± 47.1	0.99 ± 0.04
G-CSF (0.5μg/kg)			
1	600	562	0.94
2	601	650	1.08
3	494	425	0.86
4	731	731	1.00
5	767	784	1.02
6	498	501	1.01
Mean ± SEM	615.2 ± 46.7	608.8 ± 56.2	0.98 ± 0.03
G-CSF (5μg/kg)			
1	577	497	0.86
2	537	368	0.69
3	310	288	0.93
4	520	485	0.93
5	673	652	0.97
6	572	480	0.84
Mean ± SEM	531.5 ± 49.3	461.7 ± 50.8	0.87 ± 0.04
G-CSF (50μg/kg)			
1	592	520	0.88
2	463	376	0.81
3	478	430	0.90
4	307	250	0.81
5	484	410	0.85
6	385	295	0.77
Mean ± SEM	451.5 ± 39.6	380.2 ± 39.6	0.84 ± 0.02
G-CSF (250μg/kg)			
	578	424	0.73
	501	401	0.80
	507	380	0.75
	465	412	0.89
	380	341	0.90
	401	347	0.87
Mean ± SEM	472 ± 29.9	384.2 ± 14.0	0.82 ± 0.03

Right ON, under light condition; Right OFF, under dark condition.

administration of G-CSF. As G-CSF has been reported to accelerate angiogenesis in limb and cardiac models of ischemic injury (Minatoguchi *et al.*, 2004), we sought to determine its impact on neovascularization in our permanent focal cerebral infarction model. Compared with PBS-treated controls (Fig. 2A), increased neovasculature at the border of the MCA and ACA cortex (staining with TTC demarcates viable/non-viable tissue and carbon black was used to visualize vessels) was observed in animals treated with G-CSF (50 μg/kg, Fig. 2B). Assessment of the angiographic score confirmed the impression of increased neovasculature in animals treated with G-CSF, compared with the group receiving PBS (Fig. 2C; $P < 0.05$).

Next, we investigated possible neuroprotective properties of G-CSF after stroke. Analysis of the infarcted/surviving area 3 days after stroke was evaluated in animals treated with PBS (Fig. 2D) or G-CSF (50 μg/kg, Fig. 2E) based on TTC staining; there was no effect of G-CSF treatment compared with controls receiving PBS (Fig. 2F). Thus, G-CSF did not impact on the viability of 'at-risk' tissue in the

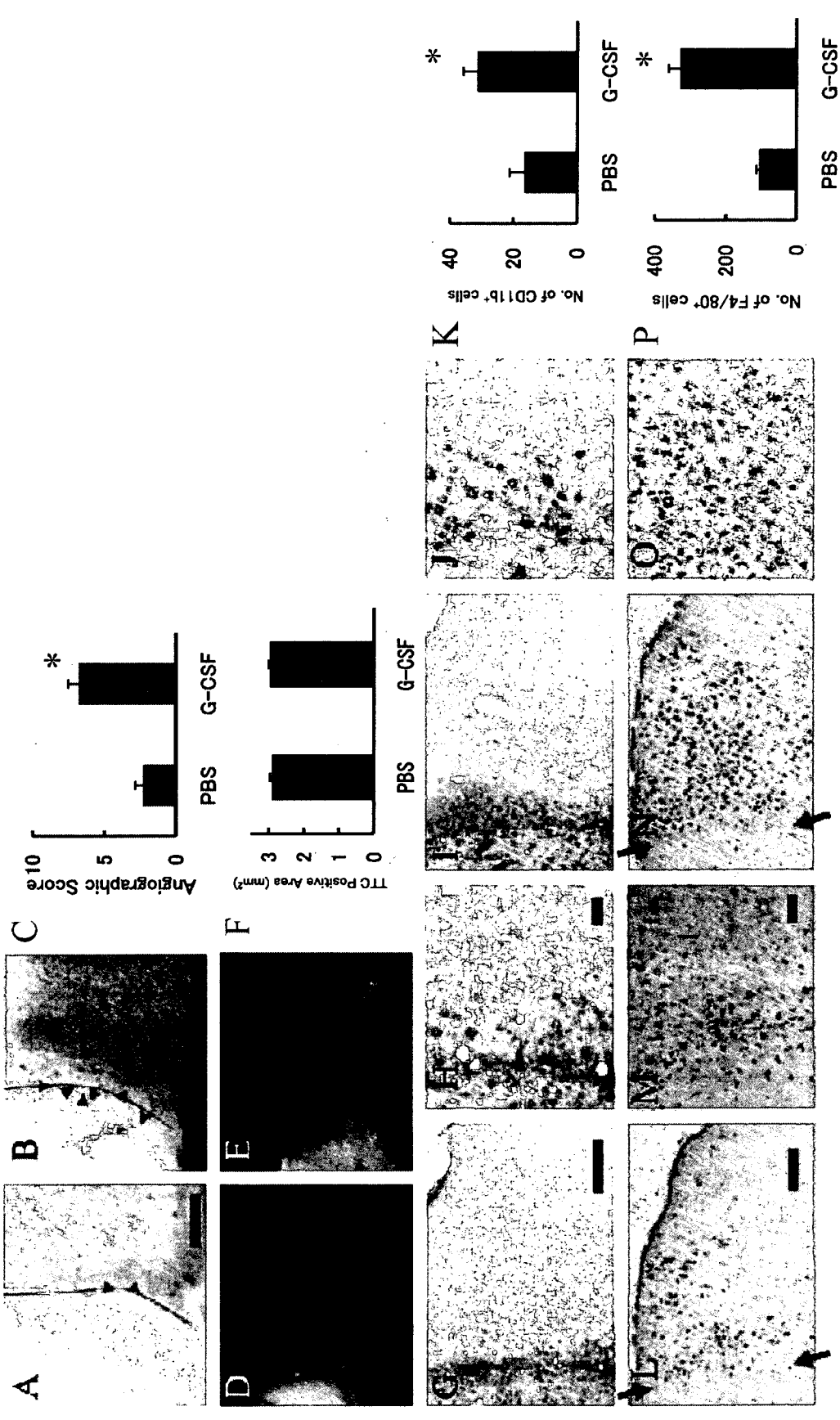

FIG. 2. Administration of granulocyte colony-stimulating factor (G-CSF) after stroke enhances the inflammatory response. (A–C) On day 3 after stroke, mice were infused with carbon black ink. Compared with mice treated with phosphate-buffered saline (PBS) (A), increased neovascularization was observed at the border between anterior cerebral artery (ACA) and middle cerebral artery (MCA) regions in mice treated with G-CSF (B). Representative micrographs are shown. The angiographic score (see Materials and methods) showed increased neovascularization ($n = 6$ per group) in mice treated with G-CSF post-stroke compared with controls (PBS). (D–F) There was no difference in the 2,3,5-triphenyltetrazolium (TTC)-positive ACA area at the exact center of forebrain comparing post-stroke animals treated with G-CSF (E) and controls/PBS (D). Sections from each animal were subjected to statistical analysis using Student's *t*-test ($n = 6$ animals per group; F). (G–K) CD11b-positive cells were visualized in the ACA area in tissue from post-stroke animals treated with PBS (G, lower magnification; H, higher magnification) or G-CSF (I, lower magnification; J, higher magnification). Sections from each animal were evaluated ($n = 6$ animals per group) and the average number of CD11b-positive cells per high power field is shown in each of the two groups (K). (L–P) F4/80-positive ($F4/80^+$) activated macrophages/microglia in mice treated with PBS were relatively limited to the area close to the border of infarcted tissue (L, lower magnification; M, higher magnification). However, an expanded area and increased density of $F4/80^+$ cells was observed after administration of G-CSF (N, lower magnification; O, higher magnification). The total number of $F4/80^+$ activated macrophages/microglia in the viable ACA area identified on the section at exact center of forebrain was quantified ($n = 6$ per group) (N). Scale bars: 0.2 mm (A), 1 mm (D), 0.3 mm (G and L) and 30 μm (H and M). $^*P < 0.05$ vs. PBS. Arrowheads (A and B) indicate microvessels at the border of the MCA and ACA cortex (red line). Arrows (L and N) indicate the border of infarcted tissue (left side, stroke MCA area; right side, viable ACA area).

immediate post-stroke period (up to 3 days), although there was a long-term effect on brain atrophy (evaluated at 35 days).

Granulocyte colony-stimulating factor enhances the inflammatory response after stroke

Further studies were performed to analyse the apparent dichotomy between G-CSF-mediated enhancement of neovascularization of the ischemic territory post-stroke vs. increased cerebral atrophy and lack of improvement in behavioral testing. We focused our studies on the inflammatory response. Compared with PBS-treated mice (Fig. 2G, lower magnification; Fig. 2H, higher magnification), increased accumulation of CD11b-positive inflammatory cells, including monocytes and granulocytes (Campanella *et al.*, 2002), was observed in G-CSF-treated mice (50 μg/kg) at the border of the infarcted area (Fig. 2I, lower magnification; Fig. 2J, higher magnification). Quantitative analysis ($n = 6$ each) revealed a significant difference in the number of infiltrating CD-11b-positive cells (Fig. 2K; $P < 0.05$). These results led us to evaluate the presence of activated macrophages/microglia in ischemic lesions, as the latter are known to enhance brain damage after stroke (Mabuchi *et al.*, 2000). Although F4/80$^+$ activated macrophages/microglia were observed in the viable (i.e. non-ischemic) ACA area following treatment with PBS (Fig. 2L, lower magnification; Fig. 2M, higher magnification), increased numbers of F4/80$^+$ macrophages/microglia were observed in post-stroke animals treated with G-CSF (Fig. 2N, lower magnification; Fig. 2O, higher magnification). F4/80$^+$ activated macrophages/microglia in post-stroke mice treated with PBS were principally limited to the area close to the border of the infarcted tissue. In contrast, F4/80$^+$ cells in post-stroke mice treated with G-CSF were observed in a broad area and at higher density in the ACA territory. The total number of F4/80$^+$ cells in a section at the exact center of the forebrain was quantified ($n = 6$ each); a significant increase in F4/80$^+$ activated macrophages/microglia was observed in G-CSF-treated mice, compared with controls receiving PBS post-stroke (Fig. 2P; $P < 0.05$).

Administration of granulocyte colony-stimulating factor 1 h after stroke also induces brain atrophy

As the experimental protocol for the above studies involved G-CSF treatment starting 24 h after stroke, it was important to vary our protocol. For this purpose, we also administered G-CSF within 1 h of stroke (Fig. 3A, $n = 6$ each) or performed continuous treatment for up to 7 days (Fig. 3B, $n = 6$ each). Our results demonstrate induction of brain atrophy in post-stroke animals treated with G-CSF subjected to either of these protocols compared with PBS-treated controls.

To exclude the immune response stimulated by human recombinant G-CSF in mice, various doses of mouse recombinant G-CSF were administered and the effect was determined ($n = 6$ each dose). We found significant brain atrophy with administration of lower doses (0.5 and 5 μg/kg) of recombinant murine G-CSF. As the survival rate was only 50% (three mice dead out of six) with administration of a higher dose (50 μg/kg), the group was excluded from this analysis.

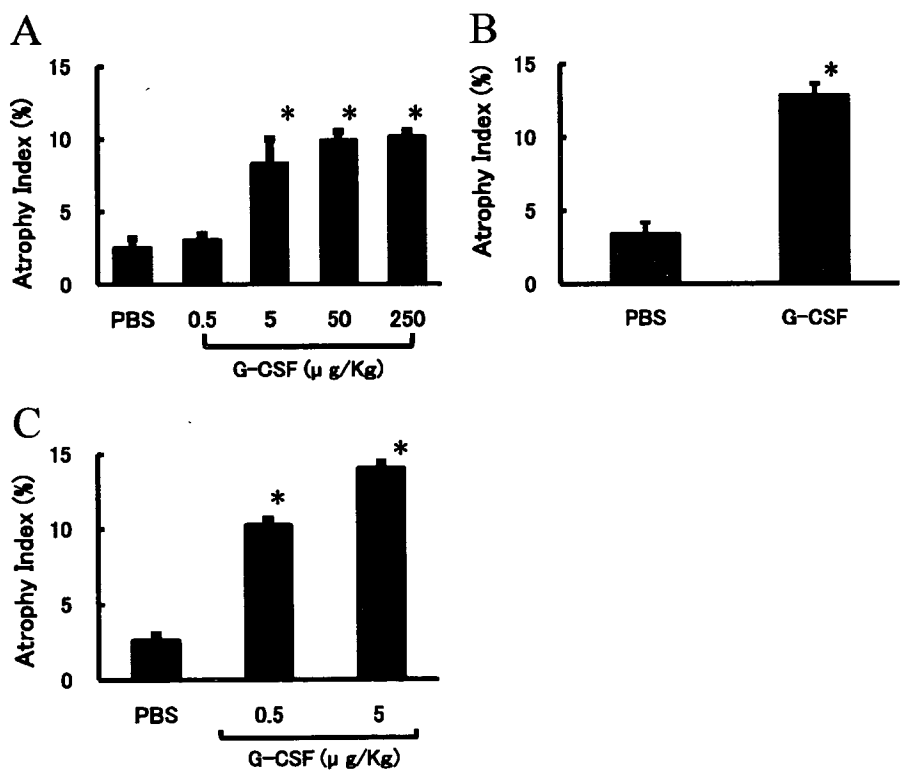

FIG. 3. Effect of granulocyte colony-stimulating factor (G-CSF) on brain atrophy. (A) G-CSF or phosphate-buffered saline (PBS) was administered 1 h after stroke and brains were evaluated grossly on day 35 post-stroke. (B) Continuous administration of G-CSF or PBS starting at 1 h post-stroke for 7 days was also tested. (C) Mouse recombinant G-CSF was administrated at the indicated dose and was found to increase the atrophy index. In each case, $n = 6$ per group. *$P < 0.05$ vs. PBS.

Discussion

Our results demonstrate that, in a murine permanent focal cerebral infarction model, administration of G-CSF, either human or murine recombinant, post-stroke is associated with enhanced brain atrophy.

In order to evaluate experimental treatments for stroke, reproducible induction of cerebral ischemia/infarction is a prerequisite. Previously, we developed a stroke model using SCID mice (Taguchi *et al.*, 2004) that proved suitable for quantification of the effect of cell therapy on neurogenesis, neovessel formation and neural function. In the current study, we have applied this stroke model to CB-17 mice and found it to provide highly reproducible data.

Granulocyte colony-stimulating factor is known to mobilize EPCs from bone marrow (Willing *et al.*, 2003) and accelerate angiogenesis (Bussolino *et al.*, 1991). Clinical studies have demonstrated that administration of G-CSF has beneficial effects in patients with acute myocardial infarction, including promotion of neovascularization and improvement of perfusion (Kuethe *et al.*, 2004). In addition, G-CSF has been shown to display neuroprotective properties in a rodent model (Schabitz *et al.*, 2003). Based on these observations, G-CSF has been tested in animal models of transient cerebral ischemia and beneficial effects have been reported (i.e. reduced infarct volume and enhanced functional recovery) (Schabitz *et al.*, 2003; Shyu *et al.*, 2004; Gibson *et al.*, 2005). In the current study, we employed a permanent cerebral infarction (i.e. stroke) model, rather than a model of transient ischemia, to investigate the effects of G-CSF.

In addition to its effects on EPCs, G-CSF is known to mobilize granuloctyes from the bone marrow, and these granulocytes have been shown to become associated with endothelia and accumulate in the ischemic brain (Justicia *et al.*, 2003). These observations suggested the possibility that G-CSF might augment the inflammatory response consequent to ischemic tissue damage by promoting recruitment and activation of neutrophils and mononuclear-derived cells (blood monocytes, monocyte-derived macrophages and microglia) (Zawadzka & Kaminska, 2005). Consistent with this concept, accumulation of CD11b-positive inflammatory cells at the border of the infarcted area was observed after treatment with G-CSF. Furthermore, a striking increase in the number of F4/80$^+$ activated macrophages/microglia was observed in non-ischemic surviving tissue (adjacent to the infarct) subsequent to administration of G-CSF. The inflammatory response after stroke has been shown to have both positive and negative effects on tissue repair (Fontaine *et al.*, 2002). Our results indicated that the balance of these inflammatory mechanisms on stroke outcome in the mouse using a permanent ischemia model and following administration of G-CSF is negative.

It would appear that the current work contradicts previous studies showing a positive effect of G-CSF after myocardial ischemia (Minatoguchi *et al.*, 2004). This apparent discrepancy may be explained, at least in part, by differences in brain and cardiac vasculature. Non-ischemic brain is protected from the systemic inflammatory response by an intact blood–brain barrier composed of endothelia joined by tight junctions. Thus, invasion of the central nervous system by activated inflammatory cells is largely prevented and the neural system functions within a relatively protected microenvironment, with respect to the inflammatory response (Neumann, 2000). However, stroke disturbs the integrity of the blood–brain barrier. We propose that a combination of impaired function of the blood–brain barrier in the context of G-CSF-induced augmentation of the inflammatory response in ischemic tissue contributes to the observed brain atrophy. Although activated inflammatory cells are known to participate in both the injurious and healing processes (Minatoguchi *et al.*, 2004), our results indicate an overall negative effect on neural function and neurogenesis following treatment with G-CSF in the post-stroke period.

In contrast to G-CSF, EPO had beneficial effects after stroke in the current model. Such positive effects are consistent with previous reports (Bernaudin *et al.*, 1999; Bahlmann *et al.*, 2004; Bartesaghi *et al.*, 2005; Kretz *et al.*, 2005) demonstrating that EPO promotes mobilization of EPCs (Bahlmann *et al.*, 2004), has angiogenic (Jaquet *et al.*, 2002) and neuroprotective properties (Bartesaghi *et al.*, 2005), and accelerates regeneration (Kretz *et al.*, 2005).

Taken together, our results indicate that administration of G-CSF after stroke results in an exaggerated inflammatory response, both at the border of the ischemic region and also in non-ischemic brain tissue, and that this is associated with brain atrophy and poor neural function. Thus, we suggest that a cautious approach should be taken in applying results of studies with G-CSF in the peripheral circulation (i.e. limb and cardiac ischemia) to the setting of cerebral ischemia. In a more general context, it is possible that agents with pro-inflammatory properties will prove less useful as therapeutic agents in cerebral ischemia in view of the above observations.

Acknowledgements

This work was partially supported by a Grant-in-Aid for Scientific Research from the Ministry of Health, Labour and Welfare. We would like to thank Y. Kasahara for technical assistance.

Abbreviations

ACA, anterior cerebral artery; EPC, endothelial progenitor cell; EPO, erythropoietin; F4/80$^+$, F4/80-positive; G-CSF, granulocyte colony-stimulating factor; MCA, middle cerebral artery; PBS, phosphate-buffered saline; SCID, severe combined immunodeficient; TTC, 2,3,5-triphenyltetrazolium.

References

Asahara, T., Murohara, T., Sullivan, A., Silver, M., van der Zee, R., Li, T., Witzenbichler, B., Schatteman, G. & Isner, J.M. (1997) Isolation of putative progenitor endothelial cells for angiogenesis. *Science*, **275**, 964–967.

Bahlmann, F.H., De Groot, K., Spandau, J.M., Landry, A.L., Hertel, B., Duckert, T., Boehm, S.M., Menne, J., Haller, H. & Fliser, D. (2004) Erythropoietin regulates endothelial progenitor cells. *Blood*, **103**, 921–926.

Bartesaghi, S., Marinovich, M., Corsini, E., Galli, C.L. & Viviani, B. (2005) Erythropoietin: a novel neuroprotective cytokine. *Neurotoxicology*, **26**, 923–928.

Bernaudin, M., Marti, H.H., Roussel, S., Divoux, D., Nouvelot, A., MacKenzie, E.T. & Petit, E. (1999) A potential role for erythropoietin in focal permanent cerebral ischemia in mice. *J. Cereb. Blood Flow Metab.*, **19**, 643–651.

Bussolino, F., Ziche, M., Wang, J.M., Alessi, D., Morbidelli, L., Cremona, O., Bosia, A., Marchisio, P.C. & Mantovani, A. (1991) In vitro and in vivo activation of endothelial cells by colony-stimulating factors. *J. Clin. Invest.*, **87**, 986–995.

Campanella, M., Sciorati, C., Tarozzo, G. & Beltramo, M. (2002) Flow cytometric analysis of inflammatory cells in ischemic rat brain. *Stroke*, **33**, 586–592.

Dzau, V.J., Gnecchi, M., Pachori, A.S., Morello, F. & Melo, L.G. (2005) Therapeutic potential of endothelial progenitor cells in cardiovascular diseases. *Hypertension*, **46**, 7–18.

Ehrenreich, H., Hasselblatt, M., Dembowski, C., Cepek, L., Lewczuk, P., Stiefel, M., Rustenbeck, H.H., Breiter, N., Jacob, S., Knerlich, F., Bohn, M., Poser, W., Ruther, E., Kochen, M., Gefeller, O., Gleiter, C., Wessel, T.C., De Ryck, M., Itri, L., Prange, H., Cerami, A., Brines, M. & Siren, A.L. (2002) Erythropoietin therapy for acute stroke is both safe and beneficial. *Mol. Med.*, **8**, 495–505.

Fontaine, V., Mohand-Said, S., Hanoteau, N., Fuchs, C., Pfizenmaier, K. & Eisel, U. (2002) Neurodegenerative and neuroprotective effects of tumor

necrosis factor (TNF) in retinal ischemia: opposite roles of TNF receptor 1 and TNF receptor 2. *J. Neurosci.*, **22**, RC216.

Gibson, C.L., Bath, P.M. & Murphy, S.P. (2005) G-CSF reduces infarct volume and improves functional outcome after transient focal cerebral ischemia in mice. *J. Cereb. Blood Flow Metab.*, **25**, 431–439.

Jaquet, K., Krause, K., Tawakol-Khodai, M., Geidel, S. & Kuck, K.H. (2002) Erythropoietin and VEGF exhibit equal angiogenic potential. *Microvasc. Res.*, **64**, 326–333.

Justicia, C., Panes, J., Sole, S., Cervera, A., Deulofeu, R., Chamorro, A. & Planas, A.M. (2003) Neutrophil infiltration increases matrix metalloproteinase-9 in the ischemic brain after occlusion/reperfusion of the middle cerebral artery in rats. *J. Cereb. Blood Flow Metab.*, **23**, 1430–1440.

Kimble, D.P. (1968) Hippocampus and internal inhibition. *Psychol. Bull.*, **70**, 285–295.

Kretz, A., Happold, C.J., Marticke, J.K. & Isenmann, S. (2005) Erythropoietin promotes regeneration of adult CNS neurons via Jak2/Stat3 and PI3K/AKT pathway activation. *Mol. Cell Neurosci.*, **29**, 569–579.

Kuethe, F., Figulla, H.R., Voth, M., Richartz, B.M., Opfermann, T., Sayer, H.G., Krack, A., Fritzenwanger, M., Hoffken, K., Gottschild, D. & Werner, G.S. (2004) Mobilization of stem cells by granulocyte colony-stimulating factor for the regeneration of myocardial tissue after myocardial infarction. *Dtsch. Med. Wochenschr.*, **129**, 424–428.

Mabuchi, T., Kitagawa, K., Ohtsuki, T., Kuwabara, K., Yagita, Y., Yanagihara, T., Hori, M. & Matsumoto, M. (2000) Contribution of microglia/macrophages to expansion of infarction and response of oligodendrocytes after focal cerebral ischemia in rats. *Stroke*, **31**, 1735–1743.

Matsushita, K., Matsuyama, T., Nishimura, H., Takaoka, T., Kuwabara, K., Tsukamoto, Y., Sugita, M. & Ogawa, S. (1998) Marked, sustained expression of a novel 150-kDa oxygen-regulated stress protein, in severely ischemic mouse neurons. *Brain Res. Mol. Brain Res.*, **60**, 98–106.

Minatoguchi, S., Takemura, G., Chen, X.H., Wang, N., Uno, Y., Koda, M., Arai, M., Misao, Y., Lu, C., Suzuki, K., Goto, K., Komada, A., Takahashi, T., Kosai, K., Fujiwara, T. & Fujiwara, H. (2004) Acceleration of the healing process and myocardial regeneration may be important as a mechanism of improvement of cardiac function and remodeling by postinfarction granulocyte colony-stimulating factor treatment. *Circulation*, **109**, 2572–2580.

Neumann, H. (2000) The immunological microenvironment in the CNS: implications on neuronal cell death and survival. *J. Neural Transm. Suppl.*, **59**, 59–68.

Schabitz, W.R., Kollmar, R., Schwaninger, M., Juettler, E., Bardutzky, J., Scholzke, M.N., Sommer, C. & Schwab, S. (2003) Neuroprotective effect of granulocyte colony-stimulating factor after focal cerebral ischemia. *Stroke*, **34**, 745–751.

Shyu, W.C., Lin, S.Z., Yang, H.I., Tzeng, Y.S., Pang, C.Y., Yen, P.S. & Li, H. (2004) Functional recovery of stroke rats induced by granulocyte colony-stimulating factor-stimulated stem cells. *Circulation*, **110**, 1847–1854.

Taguchi, A., Soma, T., Tanaka, H., Kanda, T., Nishimura, H., Yoshikawa, H., Tsukamoto, Y., Iso, H., Fujimori, Y., Stern, D.M., Naritomi, H. & Matsuyama, T. (2004) Administration of CD34+ cells after stroke enhances neurogenesis via angiogenesis in a mouse model. *J. Clin. Invest.*, **114**, 330–338.

Tamatani, M., Matsuyama, T., Yamaguchi, A., Mitsuda, N., Tsukamoto, Y., Taniguchi, M., Che, Y.H., Ozawa, K., Hori, O., Nishimura, H., Yamashita, A., Okabe, M., Yanagi, H., Stern, D.M., Ogawa, S. & Tohyama, M. (2001) ORP150 protects against hypoxia/ischemia-induced neuronal death. *Nat. Med.*, **7**, 317–323.

Walther, T., Olah, L., Harms, C., Maul, B., Bader, M., Hortnagl, H., Schultheiss, H.P. & Mies, G. (2002) Ischemic injury in experimental stroke depends on angiotensin II. *Faseb J.*, **16**, 169–176.

Wang, L., Zhang, Z., Wang, Y., Zhang, R. & Chopp, M. (2004) Treatment of stroke with erythropoietin enhances neurogenesis and angiogenesis and improves neurological function in rats. *Stroke*, **35**, 1732–1737.

Weaver, C.H., Buckner, C.D., Longin, K., Appelbaum, F.R., Rowley, S., Lilleby, K., Miser, J., Storb, R., Hansen, J.A. & Bensinger, W. (1993) Syngeneic transplantation with peripheral blood mononuclear cells collected after the administration of recombinant human granulocyte colony-stimulating factor. *Blood*, **82**, 1981–1984.

Willing, A.E., Vendrame, M., Mallery, J., Cassady, C.J., Davis, C.D., Sanchez-Ramos, J. & Sanberg, P.R. (2003) Mobilized peripheral blood cells administered intravenously produce functional recovery in stroke. *Cell Transplant.*, **12**, 449–454.

Zawadzka, M. & Kaminska, B. (2005) A novel mechanism of FK506-mediated neuroprotection: downregulation of cytokine expression in glial cells. *Glia*, **49**, 36–51.